USAARL-TECH-FR--2026-30

UNITED STATES ARMY AEROMEDICAL RESEARCH LABORATORY

The Effects of Increased Head-Supported Mass and Center of Mass Offset on the Federal Aviation Administration Hybrid III Anthropomorphic Test Device Neck Responses During Vertical Acceleration

Danielle Rhodes, Blake Johnson, Michael Schlick, Joseph Willet & B. Joseph McEntire

Notice

Qualified Requesters

Qualified requesters may obtain copies from the Defense Technical Information Center (DTIC), Fort Belvoir, Virginia 22060. Orders will be expedited if placed through the librarian or other person designated to request documents from DTIC.

Change of Address

Organizations receiving reports from the U.S. Army Aeromedical Research Laboratory on automatic mailing lists should confirm correct address when corresponding about laboratory reports.

Disposition

Destroy this document when it is no longer needed. Do not return it to the originator.

Disclaimer

The views, opinions, and/or findings contained in this report are those of the author(s) and should not be construed as an official Department of the Army position, policy, or decision, unless so designated by other official documentation. Citation of trade names in this report does not constitute an official Department of the Army endorsement or approval of the use of such commercial items.

IRB Determination and Number

N/A

REPORT DOCUMENTATION PAGE	*Form Approved* *OMB No. 0704-0188*

The public reporting burden for this collection of information is estimated to average 1 hour per response, including the time for reviewing instructions, searching existing data sources, gathering and maintaining the data needed, and completing and reviewing the collection of information. Send comments regarding this burden estimate or any other aspect of this collection of information, including suggestions for reducing the burden, to Department of Defense, Washington Headquarters Services, Directorate for Information Operations and Reports (0704-0188), 1215 Jefferson Davis Highway, Suite 1204, Arlington, VA 22202-4302. Respondents should be aware that notwithstanding any other provision of law, no person shall be subject to any penalty for failing to comply with a collection of information if it does not display a currently valid OMB control number.

PLEASE DO NOT RETURN YOUR FORM TO THE ABOVE ADDRESS.

1. REPORT DATE *(DD-MM-YYYY)*	**2. REPORT TYPE**	**3. DATES COVERED** *(From - To)*
10-08-2026	Final Report	10/1/2021-9/30/2024

4. TITLE AND SUBTITLE

The Effects of Increased Head-Supported Mass and Center of Mass Offset on the Federal Aviation Administration Hybrid III Anthropomorphic Test Device Neck Responses During Vertical Acceleration

5a. CONTRACT NUMBER

5b. GRANT NUMBER

5c. PROGRAM ELEMENT NUMBER

6. AUTHOR(S)

Rhodes, D.[1,2], Johnson, B.[1,2], Willet, J.[1,2], Schlick, M.[1,2], & McEntire, B. J.[1]

5d. PROJECT NUMBER

MO190001

5e. TASK NUMBER

5f. WORK UNIT NUMBER

7. PERFORMING ORGANIZATION NAME(S) AND ADDRESS(ES)

U.S. Army Aeromedical Research Laboratory
P.O. Box 620577
Fort Rucker, AL 36362

8. PERFORMING ORGANIZATION REPORT NUMBER

USAARL-TECH-FR--2026-30

9. SPONSORING/MONITORING AGENCY NAME(S) AND ADDRESS(ES)

U.S. Army Medical Research and Development Command
Military Operational Medicine Research Program
810 Schreider Street
Fort Detrick, MD 21702

10. SPONSOR/MONITOR'S ACRONYM(S)

USAMRDC MOMRP

11. SPONSOR/MONITOR'S REPORT NUMBER(S)

12. DISTRIBUTION/AVAILABILITY STATEMENT

DISTRIBUTION STATEMENT A. Approved for public release: Distribution unlimited.

13. SUPPLEMENTARY NOTES

[1]U.S. Army Aeromedical Research Laboratory, [2]Chenega Corporation

14. ABSTRACT

Aviator helmets are often configured with mounted technologies to give U.S. Army Warfighters a tactical advantage over the enemy. The addition of mass from helmet-mounted equipment alters the center of mass (CM) offset away from the natural balance point of the head and increases the stress experienced by the neck. As mission length and flight capabilities continue to grow and mass and CM offset demands change, researchers need to define head-supported mass (HSM) and CM offset boundaries concerning injury in severe but potentially survivable aircraft mishaps. The aim of this study was to challenge the existing U.S. Army Aeromedical Research Laboratory (USAARL) HSM Acute Neck Injury Risk Curve. For this study, the existing USAARL HSM Acute Neck Injury Risk Curve was challenged by exposing the Federal Aviation Administration (FAA) Hybrid III (HIII) anthropometric test device (ATD) with added HSM to vertical acceleration (Gz) levels that are consistent with the crashworthy seat requirements of MIL-S-58095A (canceled) (Department of Defense [DoD], 1986; DoD, 1996).

15. SUBJECT TERMS

Head-supported Mass, HSM, injury risk, cervical spine, center of gravity, helmets

16. SECURITY CLASSIFICATION OF:			**17. LIMITATION OF ABSTRACT**	**18. NUMBER OF PAGES**	**19a. NAME OF RESPONSIBLE PERSON**
a. REPORT	**b. ABSTRACT**	**c. THIS PAGE**			Amanda Hayes, MS
UNCLAS	UNCLAS	UNCLAS	SAR	46	**19b. TELEPHONE NUMBER** *(Include area code)* 334-255-6067

REPORT DOCUMENTATION PAGE (SF298)
(Continuation Sheet)

14. Abstract (continued)

The FAA-HIII ATD was encumbered with defined HSM configurations and tested on the USAARL Vertical Acceleration Tower. This assessment of the USAARL HSM Acute Neck Injury Risk Curve (McEntire & Shanahan, 1998) does not support changing the accepted injury risk threshold at this time, but further research is indicated.

Executive Summary

Aviator helmets are often configured with mounted technologies to give U.S. Army Warfighters a tactical advantage over the enemy. The addition of mass from helmet-mounted equipment alters the center of mass (CM) offset away from the natural balance point of the head and increases the stress experienced by the neck. As mission length and flight capabilities continue to grow and mass and CM offset demands change, researchers need to define head-supported mass (HSM) and CM offset boundaries concerning injury in severe but potentially survivable aircraft mishaps. The aim of this study was to challenge the existing U.S. Army Aeromedical Research Laboratory (USAARL) HSM Acute Neck Injury Risk Curve. The curve was developed to represent the relationship of the vertical CM placement as a function of head-worn mass in a severe but survivable mishap (McEntire & Shanahan, 1998). For this study, the existing USAARL HSM Acute Neck Injury Risk Curve was challenged by exposing the Federal Aviation Administration (FAA) Hybrid III (HIII) anthropometric test device (ATD) with added HSM to vertical acceleration (G_z) levels that are consistent with the crashworthy seat requirements of MIL-S-58095A (canceled) (Department of Defense [DoD], 1986; DoD, 1996). The FAA-HIII ATD was encumbered with defined HSM configurations and tested on the USAARL vertical acceleration tower.

This assessment of the USAARL HSM Acute Neck Injury Risk Curve (McEntire & Shanahan, 1998) does not support changing the accepted injury risk threshold at this time, but further research is indicated. Results indicate that HSM effects on the HIII neck are not substantially influenced under the G_z loading condition. Although it was found that mass had an influence on lower neck response and injury risk, further testing with PMHS is needed to confirm the risk of injury due to HSM and CM offset. Future ATD and PMHS studies are needed to determine how HSM and offset affect injury risk in vertical accelerative tests, including within the accepted risk area of the USAARL HSM Acute Neck Injury Risk Curve. An ATD neck that responds appropriately to accelerations when burdened with HSM should also be researched. Additionally, data collected from the U.S. Navy G_x and G_{xz} horizontal sled tests should be analyzed to validate the USAARL HSM Acute Neck Injury Risk Curve.

This page is intentionally blank.

Acknowledgments

The authors would also like to acknowledge specific integral team members who assisted with this research study. Thank you to Joseph Parish, Amanda Warren, Steven Arntzen, Lauren Watts, and Shawn Booms.

This page is intentionally blank.

Table of Contents

List of Figures

List of Tables

Table of Contents (continued)

List of Tables (continued)

Page

Table of Contents (continued)

List of Tables (continued)

This space is intentionally blank.

This page is intentionally blank.

Introduction

U.S. military helmets have become the ideal platform for mounting technologies (e.g., head-up displays, night vision goggles, helmet trackers, and communication devices) to support missions and give Warfighters an advantage over the enemy. By mounting these technologies onto helmets, the mass and center of mass (CM) location of the total head-borne system will change, which alters the stress acting on the wearer's neck and could influence the wearer's performance and injury risk in normal operational environments and in dynamic loading situations. The developers of these technologies must consider the effect of this increased stress from the additional head-supported mass (HSM) and its CM location. Additionally, through U.S. Army modernization efforts for multi-domain operations, the Army is developing the Future Long Range Assault Aircraft that will have increased airspeeds and flight maneuver capabilities over the Army's legacy helicopter fleet. These increased flight capabilities (e.g., forward speed) expose Army aircraft crewmembers to greater and different accelerative forces in helicopter mishaps than previously experienced. As mission length and flight capabilities continue to increase, and HSM and CM locations continue to change, it is important to determine the HSM and CM offset boundaries concerning injury risk in survivable mishap events.

Many studies have shown that spinal injuries reported from U.S. Army helicopter crashes were most frequent in the lumbar and cervical regions (Shanahan & Shanahan, 1989; Brozoski et al., 2020; Johnson et al., 2022). In the most recent investigation, it was estimated that 60% of the reported spinal injuries associated with fatal outcomes occurred in the cervical spine (Johnson et al., 2022). Cervical spine injuries result from either direct head/neck impacts or inertial loading to the neck (McElhaney & Meyers, 1993); the latter can be influenced by HSM and acceleration exposure. In a review of helicopter crash injuries that occurred between 1979 and 1985, Shanahan and Shanahan (1989) reported that the highest frequency of spinal fractures in the cervical and thoracic spine was at the seventh cervical vertebra (C7). This finding led to the development of the USAARL HSM Acute Neck Injury Risk Curve (McEntire & Shanahan, 1998), which indicates helmet conditions that elevate neck injury risk based on vertical CM location and head-worn mass. Maximum allowable mass requirements for the HSM Acute Neck Injury Risk Curve were developed based on Newton's second law. The development of the curve considered a neck tensile strength threshold of 4050 Newtons (N), a 35 G (where G is the standard acceleration due to earth's gravity) acceleration (at 31.4 degrees nose down, i.e., a G_{xz} vector), and a dynamic overshoot factor of 1.5. The vertical CM offset requirements were derived from the constant mass moment caused by a specific helmet and calculated about the anatomical C7/T1 juncture. The measured weight and vertical CM location of an Army aviator's Sound Protective Helmet number 4 (SPH-4), configured with the helmet tracking and targeting system for the AH-1 Cobra helicopter, was selected for this calculation as that helmet configuration represented the largest helmet mass (1.74 kilograms [kg]) and highest vertical CM (5.2 centimeters [cm]) of the Army aviator helmets used at that time. Since the SPH-4 helmet configured with the tracking/sighting system was fielded throughout the Army's AH-1 helicopter fleet, its mass-induced cervical injury risk in crash events was considered to be acceptable. A value of 11.94 cm was chosen to represent the vertical distance between the C7/T1 juncture and the tragion notch, which is representative of the Army anthropometric 95th percentile female and 85th percentile male as neck link lengths reported by Donelson & Gordon (1991). The combination of the vertical CM constant moment curve, the maximum allowable mass, and the vertical CM location of the SPH-4 helmet configured with the AH-1 Cobra tracking/targeting system were used by researchers to create the HSM Acute Neck Injury Risk Curve shown in Figure 1. The U.S. Navy (USN) and others have adopted this HSM Acute Neck Injury Risk Curve to develop their rotary-wing aircrew helmets.

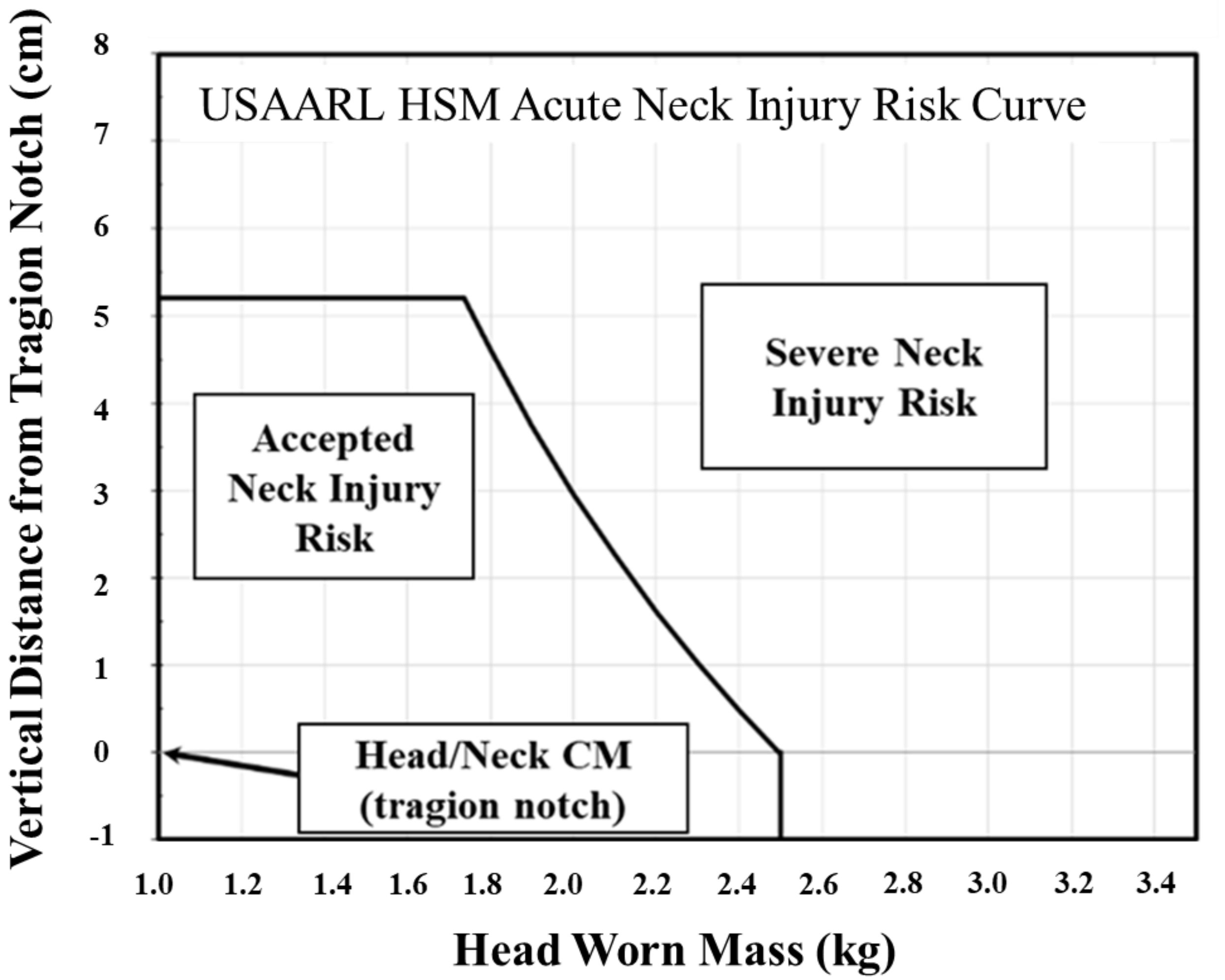

Figure 1. USAARL HSM Acute Neck Injury Risk Curve illustrating the vertical CM placement as a function of head-worn mass as reported by McEntire and Shanahan (1998).

Other studies have been conducted to examine the influence of HSM on neck injuries in vertical acceleration environments. Several studies completed by the U.S. Air Force (USAF) examined the ejection safety issues related to HSM (Knox et al., 1991). These studies, which utilized human volunteers and anthropomorphic test devices (ATDs), resulted in a USAF criterion for helmet mass and both longitudinal and vertical positioning of HSMs (the "Knox box"). The USAF, in conjunction with the Air Force Institute of Technology (AFIT), also developed neck injury criteria known as the multi-axial neck injury criteria (MANIC) (Parr et al., 2015). The MANIC was developed using existing human and PMHS datasets to establish neck injury criteria and new injury risk curves in each of the three major axes of acceleration.

However, this criterion is limited as its development was based mostly on data representative of side impacts. Additionally, the small sample sizes of the PMHS exposures in the vertical axis limited the applicability of the MANIC for predicting neck injury in vertical exposures (Parr et al., 2015).

The USN also conducted studies that identified HSM neck injury risk in ejection seat events based on: (1) measured neck loads in ATDs during dynamic testing of operational seating systems (Paskoff & Sieveka, 2004; Nichols, 2006), (2) correlation to historical mishap data, and (3) PMHS testing performed by multiple academic institutions (Lucas et al., 2008; Salzar et al., 2009; Stemper et al., 2011; Stemper et al., 2014; Yoganandan et al., 2015). The PMHS biomechanical tests subjected upper cervical spine motion segments to dynamic axial and quasi-static loads under non-destructive pure moments in flexion-extension, lateral bending, and axial rotation. Results were used by the USN as the foundation for building an anatomically based, parameterized probabilistic finite element (FE) model of the human spine in LS-DYNA (Ansys, Inc., Evanston, IL); however, further development of this model is required to ensure it is appropriately validated for use in predicting spinal injury.

Despite additional efforts to investigate and refine HSM criteria for aviators, the USAARL HSM Acute Neck Injury Risk Curve (McEntire & Shanahan, 1998) remains the benchmark for rotary-wing helmet and helmet-mounted device development efforts within the U.S. Army and USN. This report describes a Joint Program Committee 5 (JPC-5) funded research effort conducted from 2019 through 2024 by USAARL and the Naval Air Warfare Center Aircraft Division (NAWCAD) intended to substantiate the assumptions and theories employed by McEntire and Shanahan (1998). Pure vertical acceleration exposures (G_z) were conducted on the USAARL VAT and the longitudinal (G_x) and combined (G_{xz}) exposures were planned on NAWCAD's horizontal sled. Unfortunately, due to project delays, funding issues, and unavailable PMHS, the scope of this effort was reduced to ATD testing.

This report documents the ATD head and neck response test results from pure vertical acceleration exposures (G_z) on the USAARL VAT. Testing delays at NAWCAD prevented their data from being analyzed and included in this report.

This space is intentionally blank.

Methods

Controlled vertical acceleration exposures were applied to the VAT carriage configured with a 90-90-90 rigid seating system (e.g., a horizontal seat pan, vertical seat back, and horizontal foot pan). This seat geometry was previously used to assess lumbar injury tolerance and reflected a simplified, experimentally controlled seat and occupant loading configuration for vertical acceleration crash pulses. The upper bound exposure parameters in Table 1 were derived from the crashworthy seating system dynamic performance requirements of MIL-S-58095A (DoD, 1986). The pulse produced from these parameters is considered to represent a severe, but survivable, vertical acceleration pulse (Table 1). These parameters are consistent with the vertical component used by McEntire and Shanahan (1998) when the dynamic overshoot factor of 1.5 is considered. The MIL-S-58095A specifies that when the seat assembly is exposed to the vertical acceleration test conditions (Table 1), then the measured seat pan acceleration response should not exceed 23 G for more than 0.025 seconds (s) (Figure 2).

Table 1. Dynamic Vertical Accelerative Exposure Condition Required in MIL-S-58095A

Condition	**Parameter**	**MIL-S-58095A**
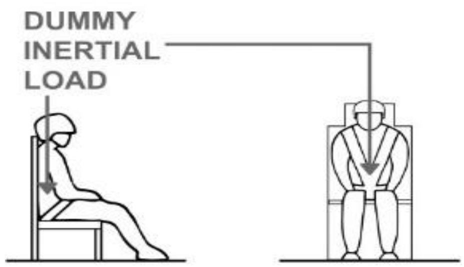	Time $(t)_1$	0.036 s
	t_2 (s)	0.051 s
	G_{min}	46
	G_{max}	51
	Change in Velocity $(\Delta V)_{min}$	42 (feet [ft]/s)
	Pitch Θ	0°
	Roll (Φ)	0°
	Yaw (Ψ)	0°

This space is intentionally blank.

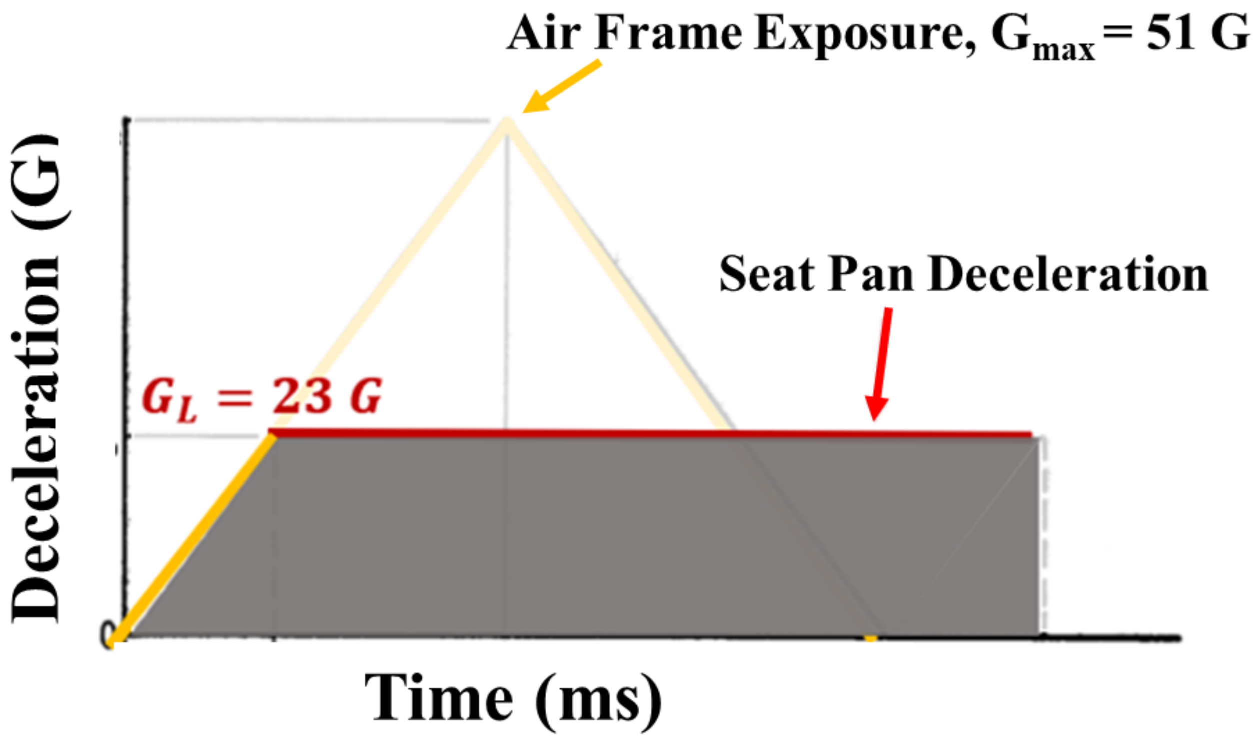

Figure 2. MIL-S-58095A requires the acceleration of the seat pan to not exceed 23 G (G_L) for more than 0.025 s.

The Federal Aviation Administration Hybrid III (FAA-HIII) ATD, with the Facial and Ocular CountermeasUres Safety (FOCUS) headform installed, was used for all testing (Figure 3). The FOCUS headform (The Humanetics Group, Farmington Hills, MI) was developed by USAARL to address the potential for face and ocular injuries and its anthropometry was copied from the USAARL standard headform used to measure head-borne mass properties (Weisenbach et al., 2020). Because the FOCUS had similar mass properties to the USAARL headform, those measurements were directly transferrable. The FAA-HIII ATD was positioned consistently within the seat and documented with a FARO ScanArm (Quantum model, FARO Technologies, Lake Mary, FL). A rotary buckle five-point restraint system without inertial reels was used to restrain the ATD. The straps were adjusted pre-test to provide 10 to 20 pounds (lb) of tension in each strap. The ATD wrists and ankles were tethered to control lateral flail during loading. After each test, the ATD was inspected for deterioration and wear in the pelvis due to repeated use.

This space is intentionally blank.

Figure 3. The FAA-HIII ATD, configured with the FOCUS headform, was positioned in a 90-90-90 rigid seating system.

An initial test was conducted without HSM to develop a baseline to compare the effects of the added HSM in subsequent tests. Helmet masses were selected along the constant moment curve developed by McEntire and Shanahan (1998) indicated by the black line numbered one through four in Figure 4. An additional mass moment curve with a 20% increase was calculated to theoretically include mass/offset of other potential helmet designs (blue line numbered five through eight) (Figure 4). The constant moment group (CMG) associated with each HSM configuration is noted in Table 2. For each HSM configuration, the total mass and CM position with respect to the tragion notch were recorded in kg and cm, respectively (Table 2). The *x*-axis CM position (CM_x) was determined by holding the *x*-axis mass moment constant (about the C7/T1 juncture) for all HSM mass levels, which means its position varied. Each HSM configuration was plotted on the FOCUS headform to illustrate the position of the weights (Figure 5).

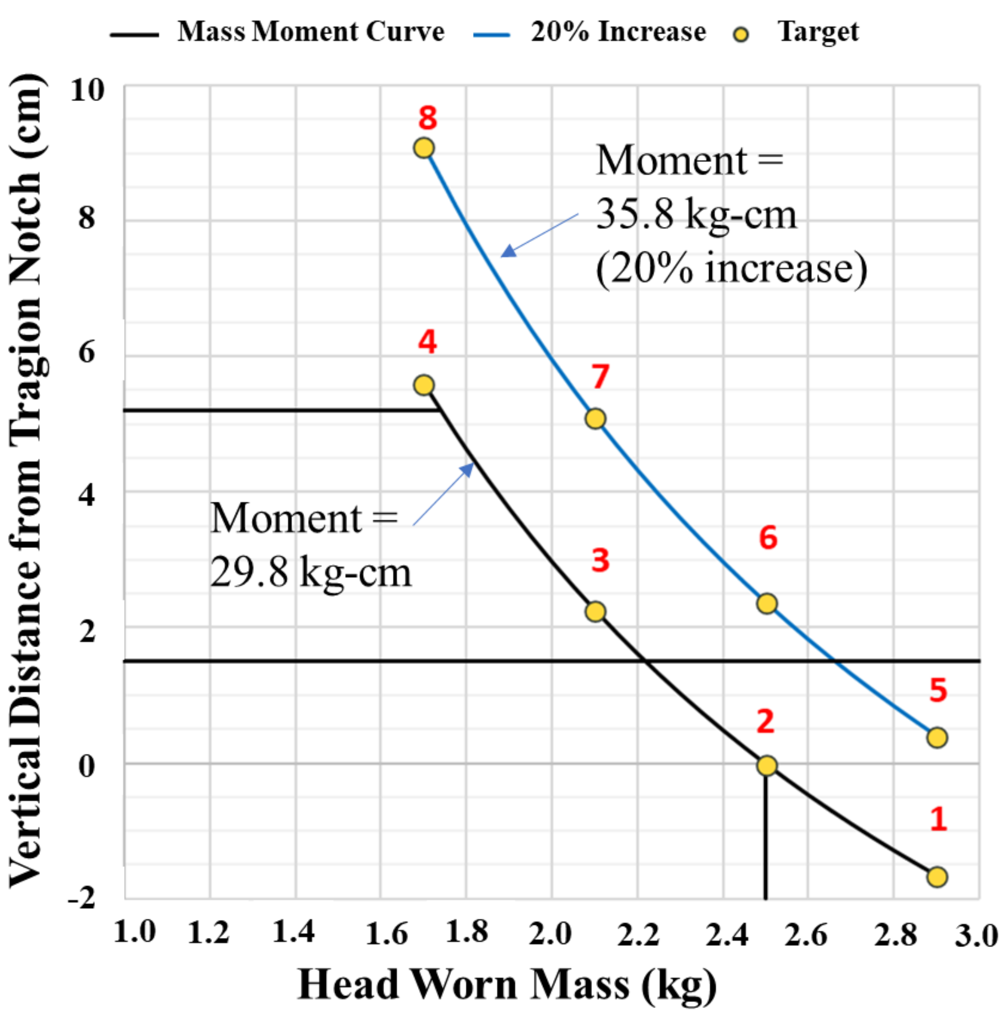

Figure 4. Four HSM configurations (labeled 1 through 4) were selected from the USAARL HSM Curves developed by McEntire and Shanahan (1998) and four additional HSM configurations were calculated by increasing the constant mass moment by 20% (labeled 5 through 8). HSM configurations labeled 1 through 4 were designated as CMG1. HSM configurations labeled 5 through 8 were designated as CMG2.

This space is intentionally blank.

Table 2. HSM Configurations for Vertical Accelerative Testing

HSM Configuration	Constant Moment Group (kg-cm)	Mass (kg)	CMx (cm)	CM_z (cm)
HSM0	0.0	NA	NA	NA
HSM1	29.8	2.91	1.61	-1.82
HSM2	29.8	2.51	2.06	-0.10
HSM3	29.8	2.11	3.27	2.12
HSM4	29.8	1.71	4.11	5.04
HSM5	35.8	2.91	1.58	-0.42
HSM6	35.8	2.51	2.00	1.56
HSM7	35.8	2.11	3.30	4.81
HSM8	35.8	1.71	3.90	9.36

Note 1. HSM0 was a baseline test with zero HSM; added mass and CG offset were not applicable (NA) for this condition.
Note 2. HSM1 through HSM4 were designated as CMG1 and HSM5 through HSM8 were designated as CMG2.

This space is intentionally blank.

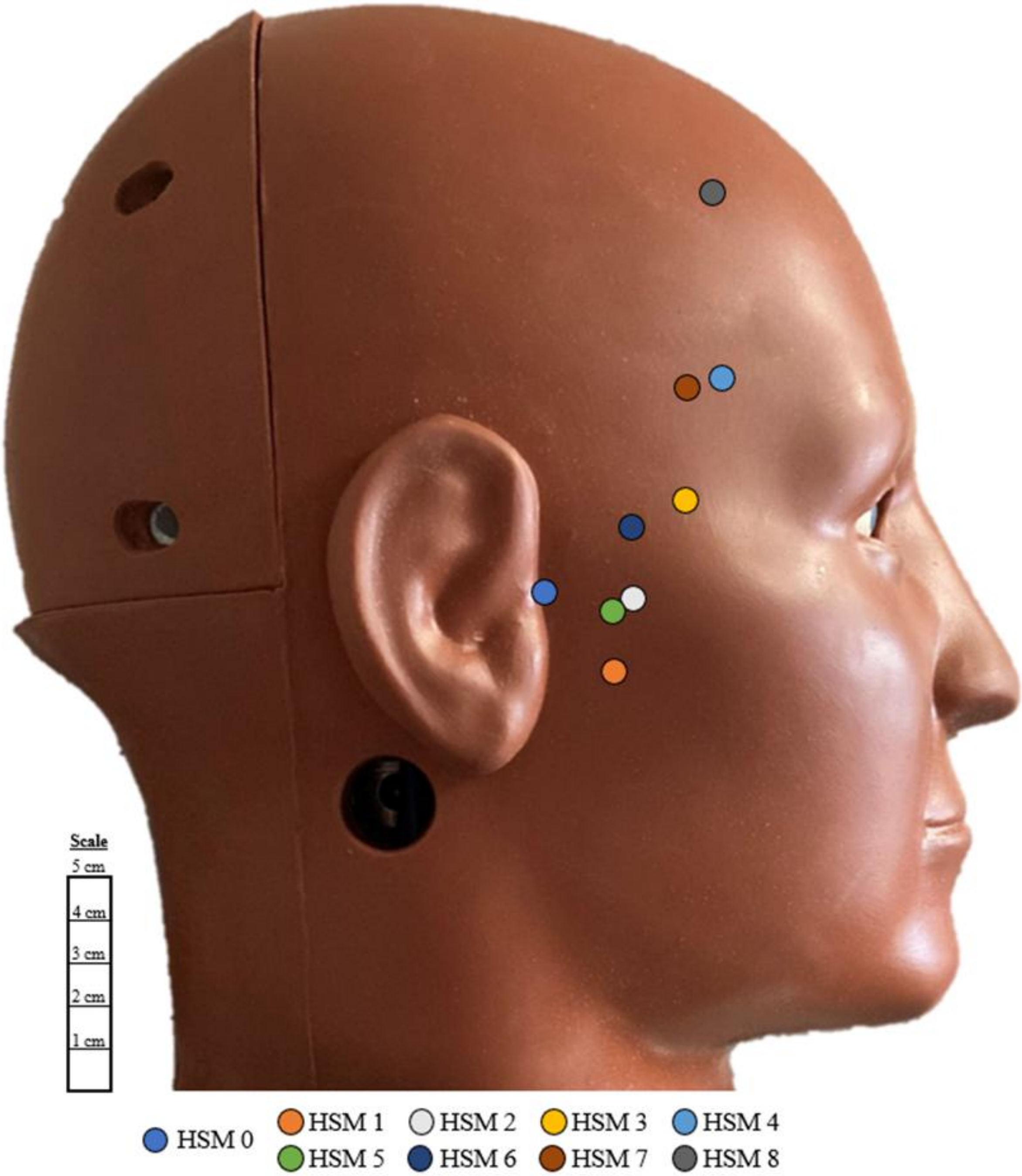

Figure 5. Each HSM configuration was plotted on the FOCUS headform to illustrate the position of the weights.

This space is intentionally blank.

The Gentex OPS-CORE Skull Mounting System (Figure 6A) was modified into a helmet mass simulation device (HMSD) following guidance from previous research by Madison (2019). This commercial product weighed approximately 0.54 kg and provided a custom fit and mounting platform for the study. The HSMD was designed to receive head-worn devices on the lateral rails (Figure 6B). The research team designed and fabricated a rail and weight system to produce the desired head-worn mass conditions (Figure 6B). These weights and CM conditions were verified by measurement on the USAARL IBPG mass properties instrument (MPI) machine prior to data collections. Preliminary fit trials onto the ATD head revealed that the retention system of the HSMD would not securely couple the headform. The HMSD retention system was consequently augmented with five hose clamps (nose, chin, forehead, nape, and crown) to securely couple the burdened HSMD to the headform during high-G exposures (Figure 7). Before the HMSD was donned for a test, all hose clamps and adjustment dials were loosened before fitting to allow the material to relax before readjustment and fitting. The three adjustment dials of the HMSD were tightened to establish the HMSD placement on the headform and provide proper alignment and positioning of the rails (Figure 6A). The nose and chin hose clamps were slipped into place and tightened to remove as much slack as possible without impacting the HMSD positioning. The triangular bracket and weights were attached to the rail at the specified locations for the desired configuration. The crown and aft hose clamps were fastened over the triangular bracket at the most posterior screw on the rail. The crown, forehead, and nape hose clamps were tightened to remove slack. To minimize inertial motion of the triangular bracket during accelerative testing, zip ties were used to secure the triangular bracket to the nose hose clamp. The FARO was used to confirm the rail positioning was within the desired criteria (± 2 degrees from the Frankfurt plane) on the left and right sides. Lastly, the crown, forehead, and nape hose clamps were tightened to the required torques: 3-pound force (lbf), 1.5-lbf, and 1-lbf, respectively.

This space is intentionally blank.

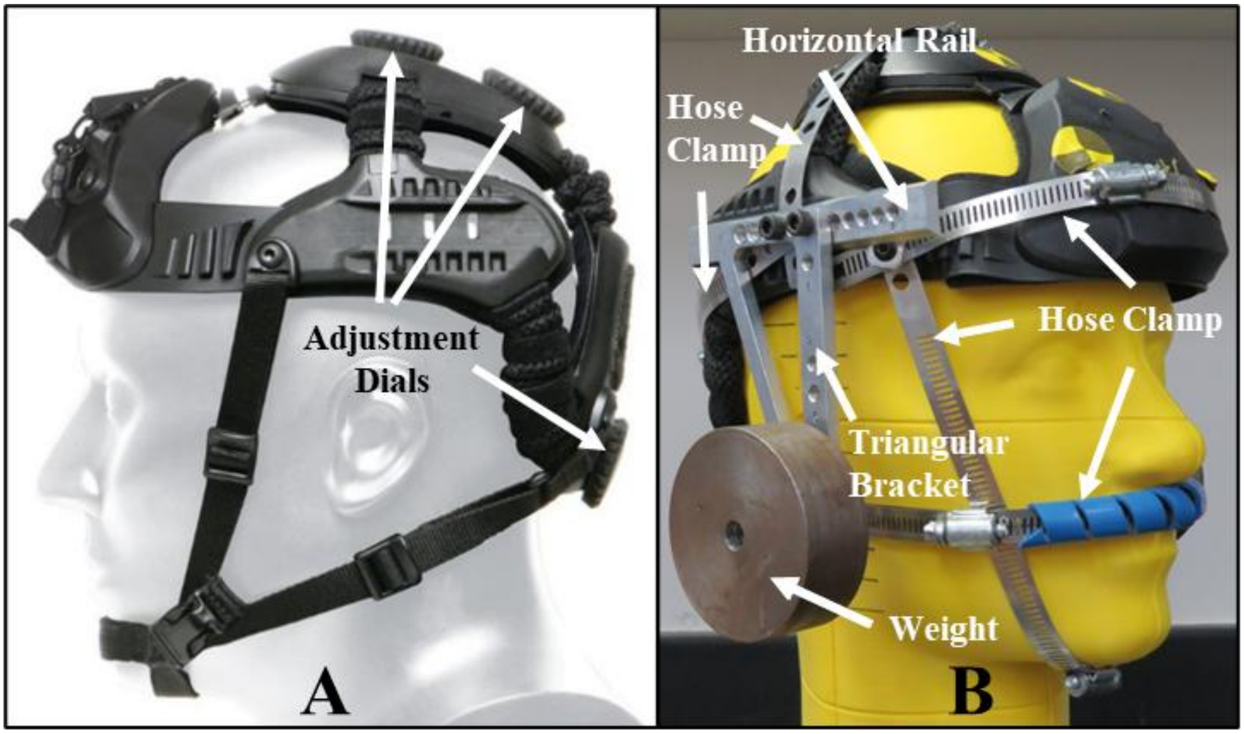

Figure 6. The lateral view of the Gentex OPS-CORE Skull Mounting System used to affix different mass configurations onto the head (A). The isometric view of the Gentex OPS-CORE Skull Mounting System with HMSD modification and weights mounted on USAARL's headform for MPI measurements (B).

This space is intentionally blank.

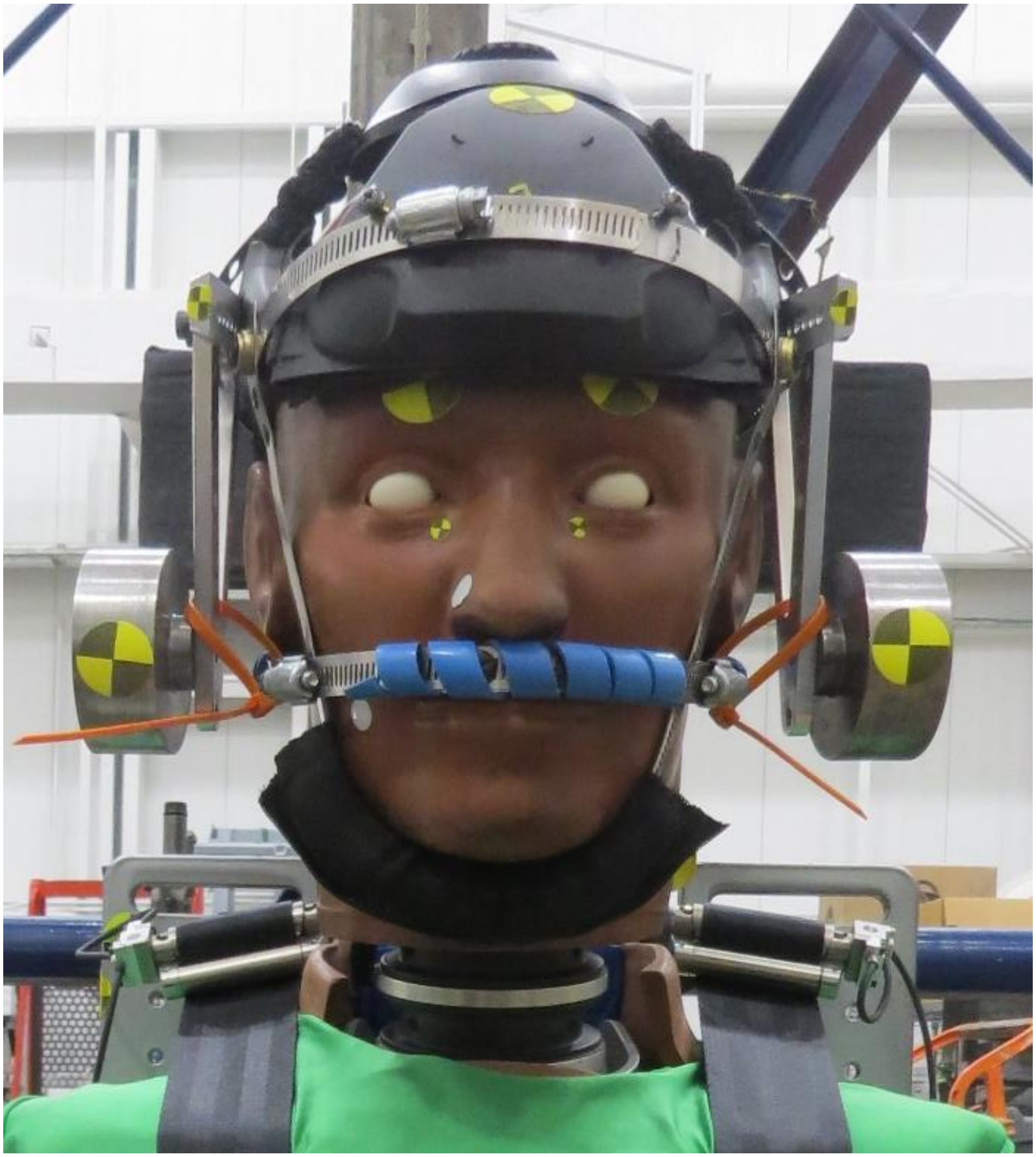

Figure 7. The research team used zip ties (orange) fastened between the triangular bracket and the nose hose clamp to minimize movement of the triangular bracket and mass relative to the FOCUS headform during vertical acceleration.

This space is intentionally blank.

All sensor data (e.g., force data, angular rate, and acceleration data) were collected at a minimum of 200,000 samples per second using a Synergy 8 data acquisition system (Hi-Techniques, Madison, WI). The impact event and overall response were documented using multiple digital high-speed video cameras at a minimum recording rate of 2000 frames per second. All sensor data acquisition and high-speed video documentation were synchronized using a common trigger signal initiated by carriage motion.

Data acquisition and reduction complied with the Society of Automotive Engineers International (SAE) J211-1, as applicable (SAE, 2007). The engineering data (e.g., acceleration, angular rate, load, displacement) collected during this study were used by researchers to assess neck responses against the existing HSM Acute Neck Injury Risk Curve. Instrumentation responses and videos were examined by the researchers to divide the event into two phases: the "thrust" phase and the "flail" phase. The thrust phase was identified as occurring between 0 and 75 milliseconds (ms) and the flail phase occurred between 76 and 180 ms. The thrust phase is considered to be the most important with respect to HSM effects due to application of seat displacement accelerations onto the seated occupant and therefore reported in the Result section and Appendix A. The flail phase generally represented the inertial rebound of the ATD, and results of this phase are reported in Appendix B. For both phases, the critical measurements included the cervical axial and anterior/posterior shear forces, and flexion/extension moment at both the upper neck load cell (UNLC) and lower neck load cell (LNLC) locations. The maximum peaks for these critical measurements in both phases were identified and tabulated.

The Neck Injury Criteria (Nij) and Beam Criteria (BC) were calculated at the thrust and flail phase (Equations 1 and 2) (Mertz & Prasad, 2000; Bass et al., 2006). The critical values used for each calculation are noted in Table 3 and 4. The Nij and BC required the raw UNLC and LNLC force channels to be separately filtered at CFC600. The Nij uses forces and moments calculated at the occipital condyles (OC), while the BC uses forces and moments calculated at the first thoracic vertebra (T1), therefore, the UNLC and LNLC signals were transformed to the OC and T1, respectively. The Nij and BC were calculated with the instantaneous measure at each time increment and the maximum reported. A Nij and BC of less than one indicates no injury.

$$Nij = \frac{F_z}{F_{zc}} + \frac{M_y}{M_{yc}} \tag{1}$$

$$BC = \frac{F_z}{F_{zc}} + \frac{M_y}{M_{yc}} \tag{2}$$

Where:

F_z is the measured load in the *z*-axis direction
F_{zc} is the critical load value for *z*-axis direction
M_y is the measured moment about the *y*-axis
M_{yc} is the critical moment value about the *y*-axis

Note that different critical values are used for force depending on the axial load being tension or compression, and different critical values for the *y*-axis moment being in flexion or extension.

Table 3. Critical Intercepts for the Nij Calculation at the UNLC Adapted From Mertz and Prasad (2000)

Measure	Critical Values
F_{zc} (Tension)	6806 N
F_{zc} (Compression)	6160 N
M_{yc} (Extension)	310 Nm
M_{yc} (Flexion)	135 Nm

Table 4. Critical Intercepts for the BC Adapted From Bass et al., 2006

Measure	Critical Values
F_z (Tension)	5660 N
F_{zc} (Compression)	5430 N
M_{yc} (Extension)	*
M_{yc} (Flexion)	141 Nm

*The BC critical value is not defined for M_{yc} (Extension). Only tension and flexion were chosen because they were the predominant injury mechanism during the PMHS tests to develop the Beam Criterion (Bass et al., 2006), therefore the extension component was ignored.

The test results were separated into thrust and flail phases. The CMG had three levels: zero-moment (CMG0, the HSM0 configuration), the initial constant moment curve (CMG1) that included HSM1 through HSM4 configurations, and the 20% increase moment curve (CMG2) that included HSM5 through HSM8 configurations (Figure 4). Upper neck and lower neck parameters F_x, F_z, M_y, and injury criteria were averaged and tabulated with their respective standard deviations (StD) for the thrust and flail phases. HSM configuration pairs selected with constant mass (Figure 8) and constant vertical offset (Figure 9) were grouped with red ovals. Percent change between the selected pairs within the ovals were calculated.

This space is intentionally blank.

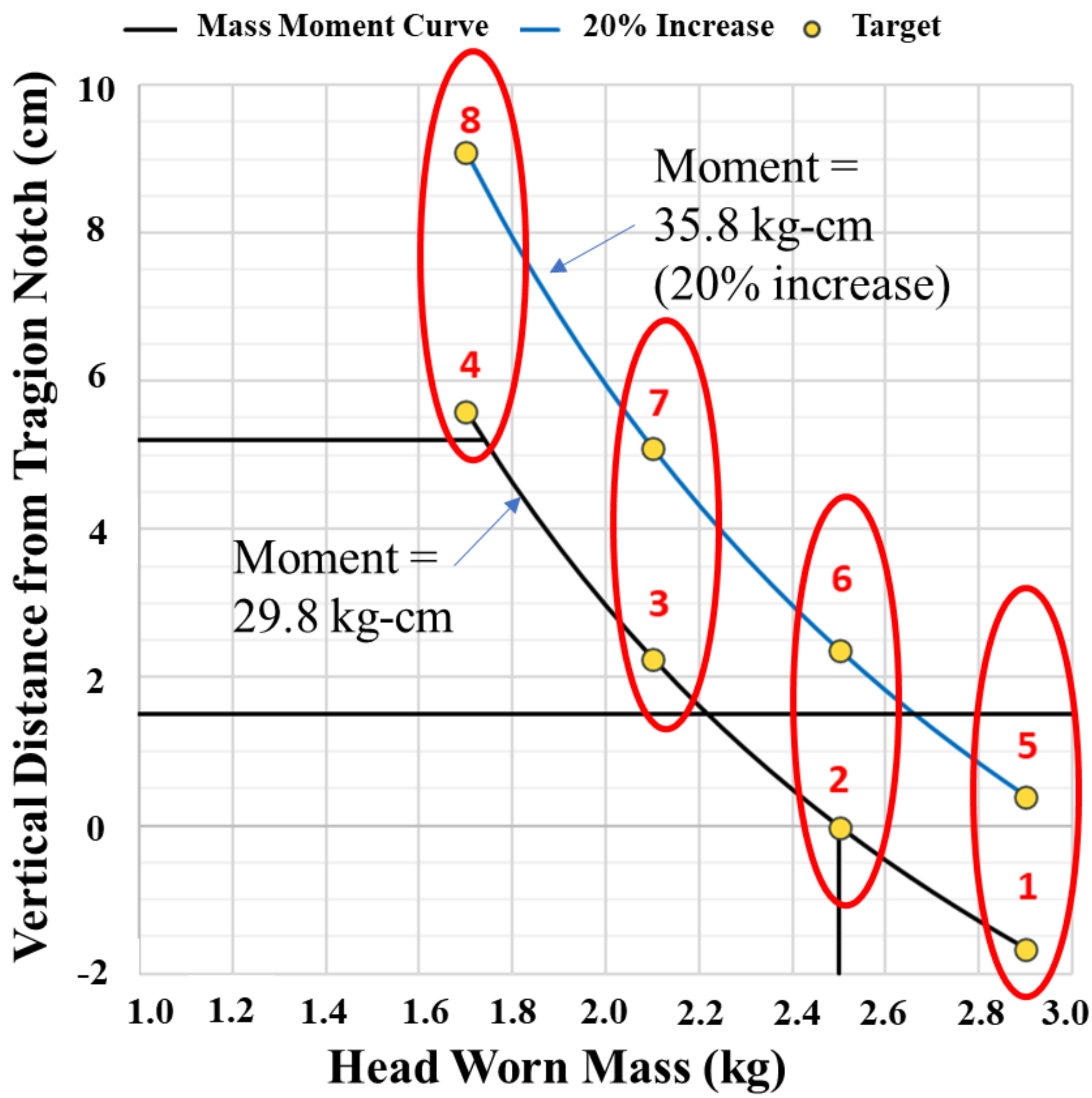

Figure 8. The constant mass pairs are indicated by the red ovals.

This space is intentionally blank.

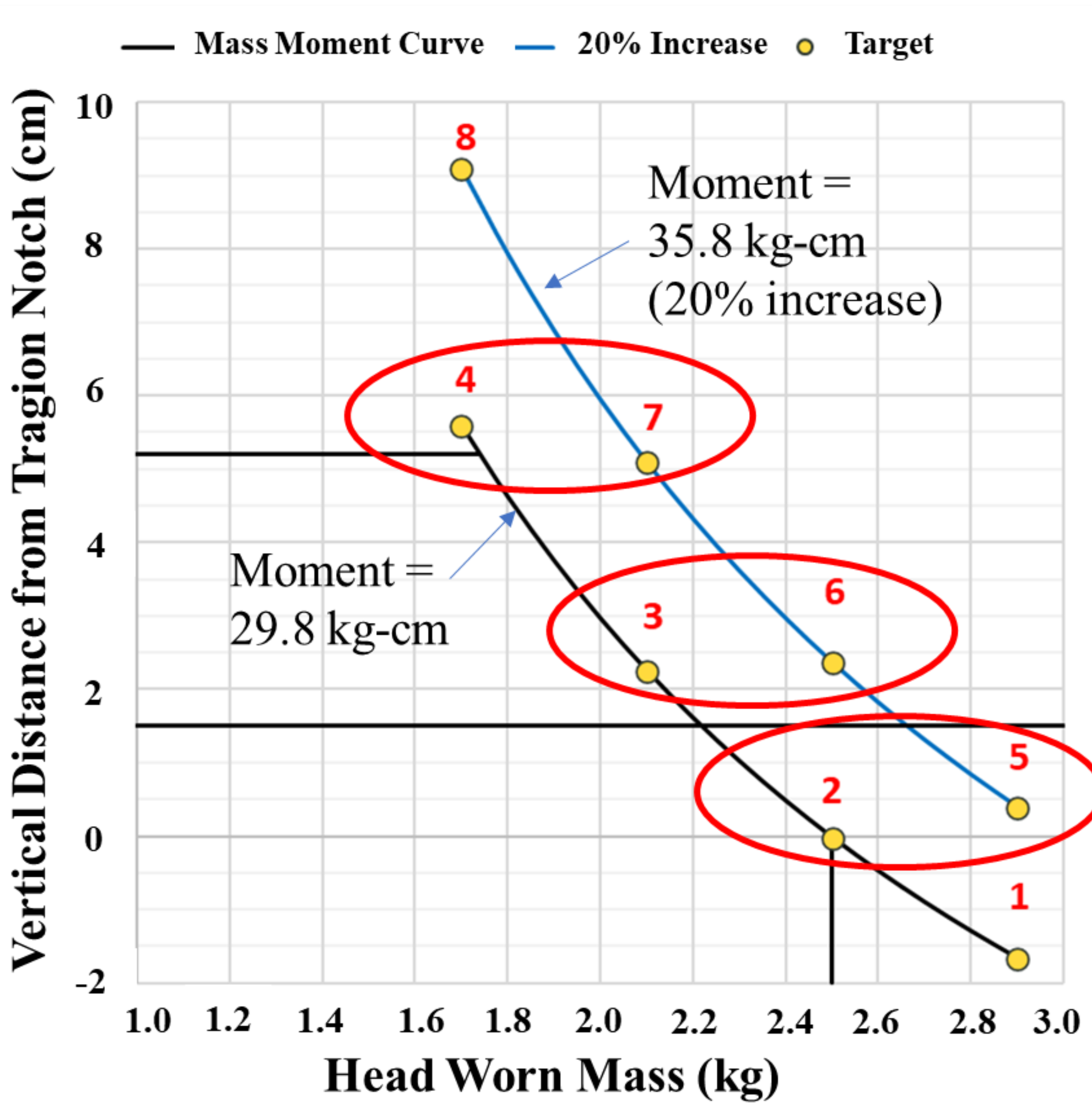

Figure 9. The vertical offset pairs are indicated by the red ovals.

One-way analyses of variance (ANOVAs) were computed for the BC, M_y, F_z, and F_x for the CMG during the thrust and flail phases. Post-hoc Tukey's Honest Significant Difference analyses were evaluated for any significant result in the independent condition variables of the HSM configuration or CMG. The total mass of the head and neck acting on the LNLC, LNLCx offset, LNLCz offset, and radial offset were tabulated. Radial offset was calculated with Equation 3. Linear regression was performed to determine if the total mass or the change in offsets were significant predictors in LNLC M_y, F_z, or F_x in both the thrust and flail phases. A linear regression trendline for each independent and dependent variable combination was performed. Additionally, data were sorted by decreasing radial offset to examine the maximum values of parameters.

$$Radial\ offset = \sqrt{LNLCx^2 + LNLCz^2} \qquad (3)$$

Results

The averaged results of the peak measurements from the conducted tests are tabulated in Appendix A. Only results from the thrust phase are presented and discussed as they are most influenced by the HSM and the focus of this effort. Results from the flail phase are included in Appendix B.

Upper and lower neck parameters F_x, F_z, and M_y were averaged and tabulated with their respective StD for each HSM test condition (three tests per HSM condition) in the thrust phase (Appendix Table A1 and A2). The CMG0, CMG1, and CMG2 are shaded gray, yellow, and blue, respectively. The maximum value for each parameter is indicated by bold red font. The Nij calculated with the UNLC data for all HSM conditions in the thrust phase was less than 1, indicating no injury (Table 5). The BC calculated with the LNLC data for all HSM conditions in the thrust phase was less than 1, indicating no injury (Table 6).

Table 5. Averaged Comparison of Nij Data for CMG0, CMG1, and CMG2 Conditions for the Thrust Phase

HSM Condition	Nij	StD
HSM0	0.806	0.01
HSM1	0.912	0.006
HSM2	0.900	0.004
HSM3	0.876	0.013
HSM4	0.836	0.008
HSM5	**0.922**	0.034
HSM6	0.888	0.049
HSM7	0.878	0.013
HSM8	0.869	0.022

Note 1. Largest Nij value of the thrust phase is in bold red font.
Note 2. CMG0 (HSM0) is shaded gray. CMG1 (HSM1 through HSM4) and CMG2 (HSM5 through HSM8) are shaded yellow and blue, respectively.

This space is intentionally blank.

Table 6. Averaged Comparison of BC Data for CMG0, CMG1, and CMG2 Conditions for the Thrust Phase

HSM Condition	BC	StD
HSM0	0.398	0.062
HSM1	0.658	0.054
HSM2	0.530	0.044
HSM3	0.615	0.025
HSM4	0.453	0.043
HSM5	**0.659**	0.068
HSM6	0.454	0.034
HSM7	0.489	0.048
HSM8	0.423	0.039

Note 1. Largest BC value of the thrust phase is in bold red font.
Note 2. CMG0 (HSM0) is shaded gray. CMG1 (HSM1 through HSM4) and CMG2 (HSM5 through HSM8) are shaded yellow and blue, respectively.

To compare the Nij and BC results between the three CMGs, the averages for each group were tabulated along with the change between groups (Table 7). An ANOVA determined that CMG was a statistically significant factor influencing the Nij value. Tukey tests were used to calculate the significance of each CMG comparison. The average Nij was 9% higher in the CMG1 condition versus the CMG0 condition ($p = 0.003$), and 10% higher in the CMG2 condition versus CMG0 ($p = 0.001$). However, there was only a 1% difference in the average Nij between CMG2 and CMG1, which was not significant ($p = 0.801$). For the LNLC, the ANOVA determined that CMG was a statistically significant factor influencing the BC values. Tukey tests determined significance of each CMG comparison. The average BC was 40% higher in the CMG1 condition versus the CMG0 condition ($p = 0.032$), and 28% higher in the CMG2 condition versus the CMG0 condition ($p = 0.156$). However, there was a -9% difference in the average BC between the CMG1 and CMG2 conditions that was not significant.

Table 7. Average Nij and BC, Standard Deviation (StD), Percent Change, and Tukey Test Results for All CMGs in the Thrust Phase

CMG Condition	Nij from UNLC		BC from LNLC	
	Average	StD	Average	StD
CMG0	0.81	0.01	0.40	0.05
CMG1	0.88	0.03	0.56	0.09
CMG2	0.89	0.03	0.51	0.10
CMG Condition Comparison	**% Change**	**Tukey Test (*p*-value)**	**% Change**	**Tukey Test (*p*-value)**
CMG1 to CMG0	9%	0.003	40%	0.032
CMG2 to CMG0	10%	0.001	28%	0.156
CMG2 to CMG1	1%	0.801	-9%	0.156

The individual components used to predict upper neck injury (UNLC M_y, F_z, and F_x) were further analyzed. In the thrust phase, the ANOVA followed by a post-hoc Tukey test revealed that the UNLC M_y, F_z, and F_x of the CMG1 and CMG2 conditions were statistically higher in magnitude than the CMG0 condition ($p < 0.05$), but not statistically different between the CMG1 and CMG2 conditions (Table 8). Differences between CMG0 and the added constant mass moment groups increased in magnitude by over 19% for all UNLC measures of interest. Differences between CMG1 and CMG2 were within 10% for all UNLC measures of interest.

Table 8. Average, StD, and % Change in Peak UNLC M_y, F_z, and F_x for All CMG in the Thrust Phase

CMG Condition	**M_y (N-m)**		**F_z (N)**		**F_x (N)**	
	Avg	**StD**	**Avg**	**StD**	**Avg**	**StD**
CMG0	17.32	0.50	-1182.25	70.47	352.22	3.75
CMG1	23.75	1.09	-1644.46	99.44	419.37	3.97
CMG2	25.80	2.40	-1621.14	115.24	430.53	5.87
CMG Condition Comparison	**% Change**	***p*-value**	**% Change**	***p*-value**	**% Change**	***p*-value**
CMG1 to CMG0	37%	<0.001	-39%	<0.001	19%	0.003
CMG2 to CMG0	49%	<0.001	-37%	0.001	22%	<0.001
CMG2 to CMG1	9%	0.032	1%	0.863	3%	0.451

The individual components, used to predict lower neck injury (peak LNLC M_y, F_z, and F_x) were further analyzed. In the thrust phase, the ANOVA followed by a post-hoc Tukey test revealed that the peak LNLC M_y, F_z, and F_x of CMG1 and CMG2 were statistically higher in magnitude than the CMG0 condition ($\alpha = 0.05$), but not statistically different between CMG1 and CMG2 (Table 9). Differences between CMG0 and the added constant mass moment groups increased in magnitude by over 19% for all peak LNLC measures of interest. Differences between CMG1 and CMG2 were within 2% for all peak LNLC measures of interest.

Table 9. Average, StD, and % Change in Peak LNLC M_y, F_z, and F_x for All CMG in the Thrust Phase

CMG Condition	**M_y (N-m)**		**F_z (N)**		**F_x (N)**	
	Avg	**StD**	**Avg**	**StD**	**Avg**	**StD**
CMG0	92.75	2.43	-1868.48	108.24	308.29	5.15
CMG1	123.49	4.54	-2249.48	109.42	425.75	33.18
CMG2	123.27	8.20	-2218.26	142.38	429.61	27.35
CMG Condition Comparison	**% Change**	***p*-value**	**% Change**	***p*-value**	**% Change**	***p*-value**
CMG1 to CMG0	33%	<0.001	-20%	<0.001	38%	<0.001
CMG2 to CMG0	33%	<0.001	-19%	0.001	39%	<0.001
CMG2 to CMG1	0%	0.997	1%	0.835	1%	0.621

The percent changes of the selected constant mass pairs for the UNLC and LNLC data were calculated (Table 10 and 11). A red font indicates a percent difference above ± 10% to help highlight any trends in the comparisons. Initial looks showed that the HSM4 and HSM8 comparison had the largest differences in the UNLC data during the flail phase. Significant differences ($p < 0.05$) between HSM configurations are indicated with an asterisk.

Table 10. Percent Differences of Constant Mass Pairs for UNLC Data

Parameter	HSM1 & HSM5	HSM2 & HSM6	HSM3 & HSM7	HSM4 & HSM8
Thrust Fx	-6.0%	6.0%	**11.1%**	-0.1%
Thrust Fz	-2.3%	2.4%	3.1%	2.8%
Thrust My	-0.5%	**13.2%**	**20.1%**	2.2%
Nij Thrust Max	1.1%	-1.3%	0.3%	3.9%

Note. Percent differences larger than ± 10% are in bold red font.

Table 11. Percent Differences of Constant Mass Pairs for LNLC Data

Parameter	HSM1 & HSM5	HSM2 & HSM6	HSM3 & HSM7	HSM4 & HSM8
Thrust Fx	**-10.5%***	3.0%	**12.4%***	0.8%
Thrust Fz	-2.6%	-2.3%	3.6%	7.0%
Thrust My	2.6%	1.6%	-5.8%	0.7%
BC Thrust Max	0.1%	**-14.3%**	**-20.5%**	-6.6%

Note. Percent differences larger than ± 10% are in bold red font.
*Statistically significant difference with *p*-value < 0.05

The percent changes of the selected vertical pairs for the UNLC and LNLC were calculated (Table 12 and 13). A bold font indicates a percent difference above ± 10%. Initial looks showed that the HSM3 and HSM6 comparison as well as the HSM4 and HSM7 comparison had the largest differences in the UNLC data during the thrust phase.

Table 12. Percent Changes of Similar Vertical Offset Pairs for UNLC Data

Parameter	HSM2 & HSM5	HSM3 & HSM6	HSM4 & HSM7
Thrust F_x	-9.1%	**14.6%***	3.4%
Thrust F_z	-0.9%	-5.9%	-2.3%
Thrust M_y	2.8%	**11.8%**	**15.2%**
Nij Thrust Max	2.4%	1.4%	5.1%

Note. Percent differences larger than ± 10% are in bold red font.
*Statistically significant difference with *p*-value < 0.05

Table 13. Percent Changes of Vertical Offset Pairs for LNLC Data

Parameter	HSM2 & HSM5	HSM3 & HSM6	HSM4 & HSM7
Thrust F_x	-2.1%	**11.1%**	**14.9%***
Thrust F_z	-0.5%	-7.7%	5.6%
Thrust M_y	6.5%	3.3%	-2.6%
BC Thrust Max	**24.3%**	**-26.2%**	8.0%

Note. Percent differences larger than ± 10% are in bold red font.
*Statistically significant difference with p-value < 0.05

Although no statistical differences were observed between the two constant moment groups (29.8 kilogram-centimeters [kg-cm] versus 35.8 kg-cm), linear regression analysis was performed to determine if the added mass or the change in LNLC offset were significant predictors in LNLC M_y, F_z, or F_x in the thrust or flail phases. Initial linear regression results produced statistically significant models but yielded high collinearity between the LNLCx and LNLCz offset (Appendix Figure A1 to A4 and Appendix Figure B1 to B2). The total mass of the head and neck and radial LNLC offset were calculated for the linear regression models (Table 14). Additionally, data were filtered by decreasing radial LNLC offset to examine the maximum values of parameters (Table 15 and 16). None of the maximum parameter values were in HSM8, which had the largest radial LNLC offset.

Table 14. Calculated Radial Offset From the LNLC

HSM Condition	Total Mass at LNLC (kg)	LNLCx Offset (cm)	LNLCz Offset (cm)	Radial LNLC Offset (cm)
HSM0	7.35	8.24	25.21	26.52
HSM1	10.26	9.85	23.39	25.38
HSM2	9.86	10.30	25.11	27.14
HSM3	9.46	11.51	27.33	29.66
HSM4	9.07	12.35	30.25	32.68
HSM5	10.26	9.82	24.79	26.67
HSM6	9.86	10.24	26.77	28.66
HSM7	9.46	11.54	30.02	32.16
HSM8	9.07	12.14	34.57	36.64

This space is intentionally blank.

Table 15. Averaged Nij Data for HSM Configurations Listed from Largest to Smallest Radial LNLC Offset for the Thrust Phase

HSM Condition	Radial LNLC offset (cm)	Nij	StD
HSM8	**10.14**	0.869	0.022
HSM4	6.50	0.876	0.013
HSM7	5.83	0.878	0.013
HSM3	3.89	0.878	0.013
HSM6	2.54	0.888	0.049
HSM1	2.43	0.912	0.006
HSM2	2.06	0.900	0.004
HSM5	1.63	**0.922**	0.034
HSM0	0	0.806	0.010

Note 1. Largest values of each parameter are in bold red font.
Note 2. CMG0 (HSM0) is shaded gray. CMG1 (HSM1 through HSM4) and CMG2 (HSM5 through HSM8) are shaded yellow and blue, respectively.

Table 16. Averaged BC Data for HSM Configurations Listed from Largest to Smallest Radial LNLC offset for the Thrust Phase

HSM Condition	Radial LNLC offset (cm)	BC	StD
HSM8	**10.14**	0.423	0.039
HSM4	6.50	0.453	0.043
HSM7	5.83	0.489	0.048
HSM3	3.89	0.615	0.025
HSM6	2.54	0.454	0.034
HSM1	2.43	0.658	0.054
HSM2	2.06	0.530	0.044
HSM5	1.63	**0.659**	0.068
HSM0	0	0.398	0.922

Note 1. Largest values of each parameter are in bold red font.
Note 2. CMG0 (HSM0) is shaded gray. CMG1 (HSM1 through HSM4) and CMG2 (HSM5 through HSM8) are shaded yellow and blue, respectively.

This space is intentionally blank.

The thrust phase LNLC M_y model was found to have the highest R^2 value (0.851), followed by the LNLC F_x (0.785), and the LNLC F_z (0.585). The total mass and radial LNLC offset coefficients were found to be statistically significant with *p*-values less than 0.001. In all three models, the total mass coefficient was statistically significant ($p < 0.001$) whereas the radial LNLC offset was not ($p > 0.05$) (Table 17).

Table 17. Thrust Phase Linear Regression Model Results for the Dependent Variables

Thrust Phase	**LNLC M_y** ($R^2 = 0.851$; *p*-value < 0.001)		**LNLC F_z** ($R^2 = 0.585$; *p*-value < 0.001)		**LNLC F_x** ($R^2 = 0.785$; *p*-value < 0.001)	
	Coefficient	***p*-value**	**Coefficient**	***p*-value**	**Coefficient**	***p*-value**
Constant	-8.196	0.564	-825.141	0.026	-88.310	0.215
Total Mass	12.806	<0.001	-153.311	<0.001	50.498	<0.001
Radial LNLC Offset	0.262	0.333	2.503	0.706	0.941	0.479

The R^2s for each independent and dependent variable were generated to illustrate the relationship between variables in both phases (Table 18). Scatter plots and linear regression equations are reported in Figures A1 - A6. The independent variable of total mass had the largest R^2 for all three dependent variables in comparison to LNLCx, LNLCz, and radial LNLC offset for the thrust phase. For the thrust phase, resulting R^2s for total mass regression models were 0.94 for LNLC M_y, 0.81 for F_z, and 0.84 for F_x indicating moderate to high correlation. The rest of the thrust regression models for the thrust phase yielded R^2s that were less than 0.1, indicating a weak relationship.

Table 18. The R^2 of Each Independent and Dependent Variable for the Thrust Phases

Output Variable	**LNLC M_y**	**Thrust LNLC F_z**	**LNLC F_x**
Total Mass	**0.94**	**0.81**	**0.84**
LNLCx Offset	0.09	0.04	0.07
LNLCz Offset	0.02	0.07	0.02
Radial LNLC Offset	0.01	0.05	0.01

Note. Strong correlations are in bold red font.

This space is intentionally blank.

Discussion

The original USAARL HSM Acute Neck Injury Risk Curve was based on theoretical Newtonian mechanics to estimate the inertial forces and moments at the occupant's C7/T1 juncture when exposed to the combined G_x and G_z crash impact accelerations. A critical parameter used in the development of the USAARL Curve was the magnitude and direction of the acceleration condition. The decision was made to use the acceleration levels from MIL-S-58095A, the standard for crashworthy pilot seats for helicopter aircrew. Another decision was to apply a 1.5 magnification factor to the acceleration level to account for dynamic overshoot of the occupant, which was determined by reviewing dynamic sled test reports on seat performance conducted by other DoD agencies and contractors. The final and most critical decision was the selection of a currently fielded (at that time) Army aircrew helmet used as a data point to serve as a foundation of the constant mass-moment curve. The helmet configuration selected was the Sound Protective Helmet #4 (SPH-4) configured with the helmet-mounted sighting and tracking system used in the AH-1 Cobra attack helicopter. This Army rotary-wing aviator helmet configuration represented the heaviest configuration and had the highest CM location that was authorized for use at that time. That configuration established the point used to anchor the constant mass moment curve about the anatomical C7/T1 level.

This research project was designed to challenge the assumptions made in developing the USAARL Curve by conducting whole-body acceleration tests in the G_x, G_z, and the combined G_{xz} conditions of MIL-S-58095A. Only results of the USAARL G_z tests are presented and discussed as the USN test data for the G_x, and G_{xz} dynamic tests were delivered to USAARL at the end of the period of performance and have not been analyzed.

The CMG0 exposures represent a baseline reference of ATD responses without any added HSM. Two experimental CMGs were evaluated, with each group made up of four different HSM configurations. From the USAARL Acute HSM Curve that represents a 29.8 kg-cm constant moment, the curve was extrapolated by extending it above the 58 millimeter CM location cutoff and 2.5 kg mass cutoff and four discrete target masses were selected for the experiment. The selected target masses were 1.7, 2.1, 2.5. and 2.9 kg, and the respective vertical CM positions were determined by the USAARL Acute HSM Curve. Together, these four HSM conditions (HSM1 - HSM4) represented CMG1. The second experimental CMG was based on a 20% increase of the constant moment to 35.8 kg-cm. The same four target masses were used to determine the vertical CM locations of four new HSM conditions (HSM5 - HSM8) and represent CMG2. The test results and analysis indicated that both CMG1 and CMG2 upper neck and lower neck data are significantly different (higher) from the un-helmeted baseline condition (CMG0). But the upper and lower neck data between CMG1 and CMG2 were not significantly different.

This space is intentionally blank.

This finding was unexpected as we anticipated a 20% increase in the constant moment condition would result in consistent detectable differences in the transmitted neck loads. We believe this result was an artifact of the pure G_z test exposure applied, compounded by the vertical stiffness of the Hybrid III type ATD. While the ATD configuration had been modified with an FAA lumbar spine for general aviation seat crash tests, it sits in a more upright posture and is less susceptible to forward flail in the pure vertical loading condition. Additionally, the Hybrid III ATD torso is constructed with a rigid thoracic spine and the HIII neck was designed to be responsive to frontal car crash impacts, not vertical loadings. So, it is probable that the ATD upper torso's poor response to vertical impact accelerations contributed to poor sensor sensitivity to experimental variations in HSM conditions.

The experimental design of the HSM test conditions also provides opportunity for investigation of the individual effect of mass and vertical CM offset. This is illustrated in Figures 8 and 9 where HSM conditions are paired together by constant mass (Figure 8) or similar vertical CM offset (Figure 9). Four constant mass pairs exist such that each pair has the same mass configured on the HMSD, but at different vertical CM locations. The difference in mass between pairs was 0.4 kg. The intent for this design was to demonstrate a vertical CM effect by revealing the measured neck response change within each mass pair as the CMz offset position increased and to illustrate the consistency of neck response change across the mass pairs. The second opportunity paired the HSM configurations with similar CMz offset positions but with masses that were different by 0.4 kg. The intent for these pairings was the same as for the mass pairs, to reveal changes in the measured neck response associated with changing mass and to determine if the pattern was consistent across the pairs. Unfortunately, for both grouping pairs, the neck response measurement results are mixed and inconsistent (Tables 9 through 12). As discussed above, the inability to detect the influence of HSM variations on the HIII ATD's neck load cells may be attributed to the ATDs' rigidity in the vertical loading direction.

The mean Nij values calculated from the UNLC for each HSM condition were all within the Nij acceptance threshold by being less than a value of 1.0. As a baseline condition, the un-helmeted condition HSM0 resulted with a mean Nij value of 0.806 with a standard deviation of 0.01. For the helmeted conditions, HSM4 (1.7 kg, CMG1) resulted in the lowest mean Nij score of 0.836 while HSM5 (2.9 kg, CMG2) resulted in the highest mean Nij score of 0.922. Within each CMG, the Nij value increases with increasing head-borne mass condition. However, this Nij trend with head-borne mass may only be applicable to the pure G_z acceleration condition, and not the G_x or combined G_{xz} acceleration conditions.

The mean BC values calculated from the LNLC for each HSM condition were all within the BC acceptance threshold by being less than a value of 1.0. As a baseline condition, the un-helmeted condition, HSM0, resulted with a mean BC value of 0.398 and a standard deviation of 0.062. For the helmeted conditions, the largest and smallest BC values are both from CMG2 with HSM5 (2.9 kg, lowest CMz offset) being the highest BC value at 0.659 and HSM8 (1.7 kg, highest CMz offset) being the lowest BC value at 0.423. No consistent trend for the BC value is evident.

The FAA-HIII lumbar spine was designed for vertical accelerative loading; however, the neck was designed predominantly for G_x impact events. The HIII neck of the FAA-HIII was designed to flail in the automotive G_x frontal loading condition. In the G_z environment, its biofidelity is not validated and may mask the effects of HSM and location. Additionally, the straight lumbar spine positions the ATD in a more erect seating posture; therefore, the CM is located closer to the spinal axis, which likely resulted in dampened HSM effects. As a result, it is likely that the effects of HSM were underestimated in this study for the G_z environment. However, the data collected by the USN in the G_x and G_{xz} should be analyzed to examine the effects that HSM and location has on acute neck injury risk with the HIII neck.

The CM differences in the eight HSM configurations tested in this study may not have been large enough for the HIII neck to respond differently to the CMGs. The biological tissue of a PMHS would have different kinematic responses than the stiffer mechanical components of the ATD. The USAARL HSM Acute Injury Risk Curve assumes that neck injury risk is related to the mass moment placed upon the C7/T1 juncture (McEntire & Shanahan, 1996). The curves indicate that increasing the moment, whether via an increase in weight or an increase in CM offset, will increase the lower neck injury risk. The Nij indicated no injury for all HSM configurations. According to the resulting BC outcomes, both mass moment conditions, the CMG1 and CMG2 conditions were above 1, indicating an increased likelihood of injury. However, the BC assessment indicated that there was little difference between the CMG1 and CMG2 conditions even though the moment was increased by 20%. This was because there was no statistical difference between the CMG1 and CMG2 conditions for LNLC M_y or F_z. The BC was developed for combined horizontal and vertical impacts, not purely vertical. Additionally, the BC was not specifically developed for HSM. However, there are no other lower neck injury criteria recommended for the military environment to evaluate HSM (Rhodes et al., 2022). Because of the HIII neck stiff construction and lack of validation in vertical exposures, it was difficult to assess injury between different HSM configurations; therefore, it is recommended that this study be repeated with PMHS to verify injury risk with HSM and then validate injury metrics such as Nij and BC with matched-pair testing.

A CM parameter not yet addressed is the HSM CM location along the *x*-axis (fore/aft direction). The *x*-axis CM locations for the eight test configurations were intentionally selected from the USAARL Performance Curve (McEntire & Shanahan, 1998). The four selected masses (1.7, 2.1, 2.5, and 2.9 kg) were applied to the USAARL Constant Moment Curve (105.6 N-cm) to determine the target location of the longitudinal CM position for the eight HSM test configurations. While the *x*-axis CM location was ignored in the development of the original USAARL Acute Neck Injury Curve as the focus was on the G_x and combined G_{xz} acceleration conditions, this parameter may be more critical in the G_z acceleration loading condition.

This space is intentionally blank.

Further research is needed to assess how CM offset influences injury risk. Linear regression was used to determine the influence of the individual components that affect the mass moment and BC. In all models, the LNLCx and LNLCz offsets were determined to be correlated and inflated the variance within the model. As the LNLCx and LNLCz were both manipulated to create a constant mass moment over four HSM configurations, the strong correlation between the two offsets was anticipated and replaced in the regression models with the radial LNLC offset. After replacing the individual offset directions with a radial offset variable, the mass was still the only significant coefficient for all linear regression models. It is recommended that additional studies, including PMHS studies, be conducted while keeping the mass and either LNLCx or LNLCz constant to determine the effects of horizontal and vertical offset on injury risk.

Finally, a related aspect of the USAARL HSM Acute Neck Injury Risk Curve that needs updating is the terminology of injury severity used to describe relatively safe and unsafe conditions, as related to head-worn mass and vertical distance from the tragion notch (Figure 1). While these terms (i.e., acceptable and severe) are descriptive, convey meaning, and have withstood the test of time, they are imprecise and inconsistent with current safety risk assessment conventions. This issue was not an objective of the present study, but is noted as a topic for further review.

Conclusion

While this assessment of the USAARL HSM Acute Neck Injury Risk Curve (McEntire & Shanahan, 1998) does not support changing the accepted injury risk threshold at this time, further research is indicated. Results indicate that HSM effects on the HIII neck are not substantially influenced under the G_z loading condition. Although it was found that mass had an influence on lower neck response and injury risk, further testing with PMHS is needed to confirm the risk of injury due to HSM and CM offset. Future ATD and PMHS studies are needed to determine how HSM and offset affect injury risk in vertical accelerative tests, including within the accepted risk area of the USAARL HSM Acute Neck Injury Risk Curve. An ATD neck that responds appropriately to accelerations when burdened with HSM should also be researched. Additionally, data collected from the USN G_x and G_{xz} horizontal sled tests should be analyzed to validate the USAARL HSM Acute Neck Injury Risk Curve.

References

Bass, C., Donnellan, L., Salzar, R., Lucas, S., Folk, B., Davis, M., Rafaels, K., Planchak, C., Meyerhoff, K., & Ziemba, A. (2006). A new neck injury criterion in combined vertical/frontal crashes with head supported mass. *2006 International conference on the biomechanics of impact (IRCOBI)*. IRCOBI. http://www.ircobi.org/wordpress/downloads/irc0111/2006/Session2/21.pdf

Brozoski, F. T., Chancey, V. C., Licina, J. R., & McEntire, B. J. (2020). *Retrospective review of spinal injuries in U.S. Army rotary-wing mishaps: January 1990-December 2014* (Report No. USAARL-TECH-FR--2020-024). U.S. Army Aeromedical Research Laboratory.

Department of Defense (DoD). (1986) *Seat system: Crashworthy, non-ejection, aircrew, general specification for* (MIL-S-58095A [AV]) U.S. Department of Defense.

DoD. (1996). *Seat system: Crashworthy, non-ejection, aircrew, general specification for* (MIL-S-58095A [AV] Notice 1). U.S. Department of Defense.

Donelson, S. & Gordon, C. (1991). *1988 anthropometric survey of U.S. Army personnel: Pilot summary statistics* (Report No. NATICK/TR-91/040). U.S. Army Natick Research, Development and Engineering Center. https://apps.dtic.mil/sti/citations/ADA241952

Johnson, B. A., Logsdon, K. P., & McEntire, B. J. (2022). *A review of cervical spine injuries among occupants involved in rotary-wing aircraft mishaps from 1990 to 2018* [Oral presentation]. 60th Annual SAFE Symposium.

Knox, F. S., Buhrman, J. R., Perry, C. E., & Kaleps, I. (1991). *Interim head/neck criterion* [Unpublished consultation report]. Air Force Research Laboratory.

Lucas S. R., Bass C.R., Salzar R.S., Oyen M.L., Planchak C., Ziemba A., Shender B.S., & Paskoff G. (2008). Viscoelastic properties of the cervical spinal ligaments under fast strain-rate deformations. *Acta Biomaterialia*, 4, 117–125. https://doi.org/10.1016/j.actbio.2007.08.003

Madison, A. (2019). *Preliminary head-supported mass (HSM) performance guidance for dismounted Soldier environments* (Technical Memorandum No. 2019-11). U.S. Army Aeromedical Research Laboratory. (NOTE: Limited Release).

Mertz, H. J., & Prasad, P. (2000). Improved neck injury risk curves for tension and extension moment measurements of crash dummies. *Stapp Car Crash Journal, 44*, 59–75. https://doi.org/10.4271/2000-01-SC05

McElhaney, J. H., & Myers, B. S. (1993). Biomechanical aspects of cervical trauma. In A. M. Nahum & J. W. Melvin (Eds.), *Accidental Injury* (pp. 311–361). Springer. https://doi.org/10.1007/978-0-387-21787-1_15

McEntire, B. J., & Shanahan, D. F. (1998). *Mass requirements for helicopter aircrew helmets* (Report No. USAARL 98-14). U.S. Army Aeromedical Research Laboratory.

Nichols, J. P. (2006). *Overview of ejection neck injury criteria*. Proceedings of the 44th Annual SAFE Symposium (pp. 159-171). SAFE Association.

Parr, J. (2014). *A method to develop neck injury criteria to aid design and test of escape systems incorporating helmet-mounted displays* [Doctoral dissertation, Air Force Institute of Technology]. https://apps.dtic.mil/sti/tr/pdf/ADA608849.pdf

Parr, J. C., Miller, M. E., Colombi, J. M., Kabban, C. M. S., & Pellettiere, J. A. (2015). Development of a side-impact (Gy) neck injury criterion for use in aircraft and vehicle safety evaluation. *IIE Transactions on Occupational Ergonomics and Human Factors, 3*(3-4), 151–164. https://doi.org/10.1080/21577323.2015.1022283

Paskoff, G. R., & Sieveka, E. (2004). *Influence of added head mass properties on head/neck loads during standard helicopter impact conditions*. Proceedings of the 42nd Annual SAFE Association Symposium (pp. 20–40). SAFE Association.

Rhodes, D., Flath, N. L., Brown, B. A., Ballard, M. T., Williams, S. T., Robinette, A. M., Lafferty, E. L., Chancey, V. C., & McEntire, B. J. (2022). *Critical review of injury assessment reference values for application in the military environment: Volume 1* (Report No. USAARL-TECH-FR--2022-45). U.S. Army Aeromedical Research Laboratory.

Salzar, R. S., Bolton, J. R., Crandall, J. R., Paskoff, G. R., & Shender, B. S. (2009). Ejection injury to the spine in small aviators: Sled tests of manikins vs. post mortem specimens. *Aviation Space & Environmental Medicine, 80*, 621–628. https://doi.org/10.3357/ASEM.2472.2009

Shanahan D. F., & Shanahan M. O. (1989). Injury in U.S. Army helicopter crashes October 1979-September 1985. *Journal of Trauma and Acute Care Surgery*, 29(4), 415–423. https://journals.lww.com/jtrauma/citation/1989/04000/Injury_in_U_S__Army_Helicopter_Crashes_October.1.aspx

SAE International. (2007). *Instrumentation for impact test- Part 1-Electronic instrumentation* (SAE J211-1).

Stemper B. D., Yoganandan N., Paskoff G. R., Filalkowski R. J., Storvik S. G., Baisden J. L., Pintar F. A., & Shender B. S. (2011). Thoraco-lumbar spine trauma in military environments. *Minerva Orthopedica e Traumatologica, 62*(5), 397–412.

Stemper, B. D., Yoganandan, N., Baisden, J. L., Umale, S., Shah, A. S., Shender, B. S., & Paskoff, G. R. (2014). Rate-dependent fracture characteristics of lumbar vertebral bodies. *Journal of the Mechanical Behavior of Biomedical Materials, 41*, 271–279. https://doi.org/10.1016/j.jmbbm.2014.07.035

Weisenbach, C. A., Gomez, J., Daniel, R. W., & Brozoski, F. T. (2020). *Summary of available craniomaxiollofacial injury criteria for use with the FOCUS headform* (Report No. USAARL-TECH-FR--2020-019). U.S. Army Aeromedical Research Laboratory.

Yoganandan, N., Stemper, B. D., Baisden, J. L., Paskoff, G. R., & Shender, B. S. (2015). Effects of acceleration level on lumbar spine injuries in military populations. *The Spine Journal, 15*(6), 1318–1324. https://doi.org/10.1016/j.spinee.2013.07.486

This space is intentionally blank.

Appendix A. Thrust Data

Table A1. Averaged Comparison of UNLC Data for CMG1 and CMG2 Conditions for the Thrust Phase

HSM	Thrust F_x		Thrust F_z		Thrust M_y		Nij Thrust	
	N	StD	N	StD	N-m	StD	Nij	StD
HSM0	352.3	4.4	-1182.3	86.3	681.9	24.5	0.806	0.01
HSM1	417.2	13.8	-1714.8	9.8	942.1	22.7	0.912	0.006
HSM2	431.9	5.3	-1739.3	73.4	911.4	28.5	0.900	0.004
HSM3	399.5	24.5	-1604.0	29.8	923.5	78.7	0.878	0.013
HSM4	429.3	8.0	-1519.5	78.7	962.6	34.7	0.876	0.013
HSM5	392.3	3.6	**-1754.4**	36.0	937.2	38.3	**0.922**	0.034
HSM6	**457.7**	16.0	-1698.3	28.9	1032.4	125.0	0.888	0.049
HSM7	443.5	10.2	-1555.1	37.8	**1108.9**	20.9	0.878	0.013
HSM8	428.4	12.5	-1477.3	53.4	983.9	109.9	0.869	0.022

Note 1. Largest values of the flail phase are in bold red font.
Note 2. CMG0 (HSM0) is shaded gray. CMG1 (HSM1 through HSM4) and CMG2 (HSM5 through HSM8) are shaded yellow and blue, respectively.

Table A2. Averaged Comparison of LNLC Data for CMG1 and CMG2 Conditions for the Thrust Phase

HSM	Thrust F_x		Thrust F_z		Thrust M_y		BC Thrust	
	N	StD	N	StD	N-m	StD	BC	StD
HSM0	308.3	6.2	-1868.7	132.6	3651.5	117.0	0.398	0.922
HSM1	**474.2**	8.5	-2261.9	11.1	5081.2	107.6	0.658	0.054
HSM2	433.3	5.8	-2307.7	62.3	4893.0	168.6	0.530	0.044
HSM3	401.7	19.1	-2190.7	65.4	4813.4	100.5	0.615	0.025
HSM4	393.2	9.3	-2237.0	230.0	4659.5	56.0	0.453	0.043
HSM5	423.9	6.2	-2320.6	31.6	**5212.0**	121.4	**0.659**	0.068
HSM6	446.2	33.8	**-2360.7**	137.4	4973.6	339.8	0.454	0.034
HSM7	451.5	14.7	-2112.0	50.7	4536.3	287.8	0.489	0.048
HSM8	396.3	15.1	-2080.0	86.7	4691.1	90.7	0.423	0.039

Note 1. Largest values of the thrust phase are in bold red font.
Note 2. CMG0 (HSM0) is shaded gray. CMG1 (HSM1 through HSM4) and CMG2 (HSM5 through HSM8) are shaded yellow and blue, respectively.

This page is intentionally blank.

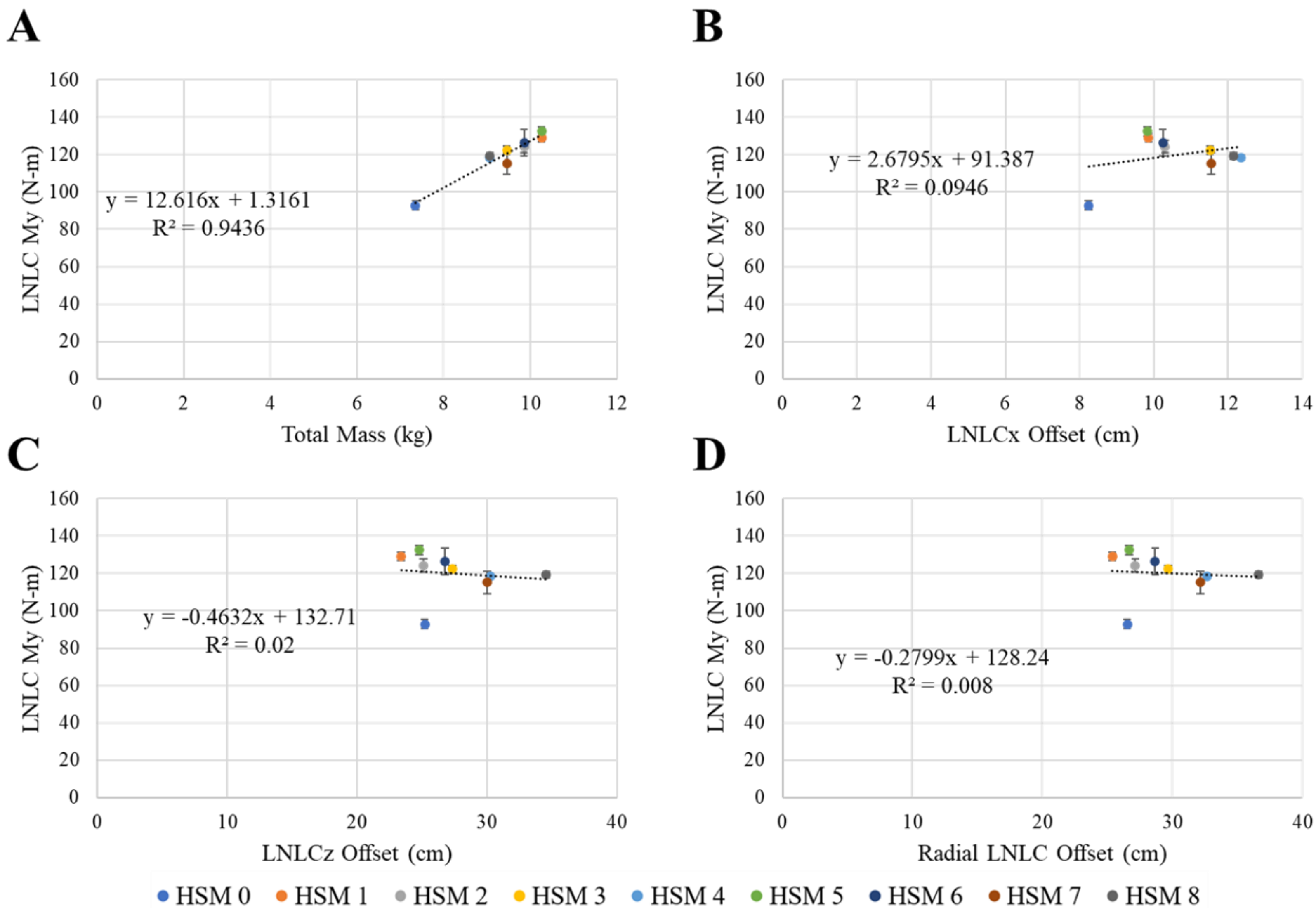

Figure A1. Scatter plots of LNLC M_y versus (A) total mass, (B) LNLCx offset, (C) LNLCz offset, and (D) radial LNLC offset in the thrust phase were produced.

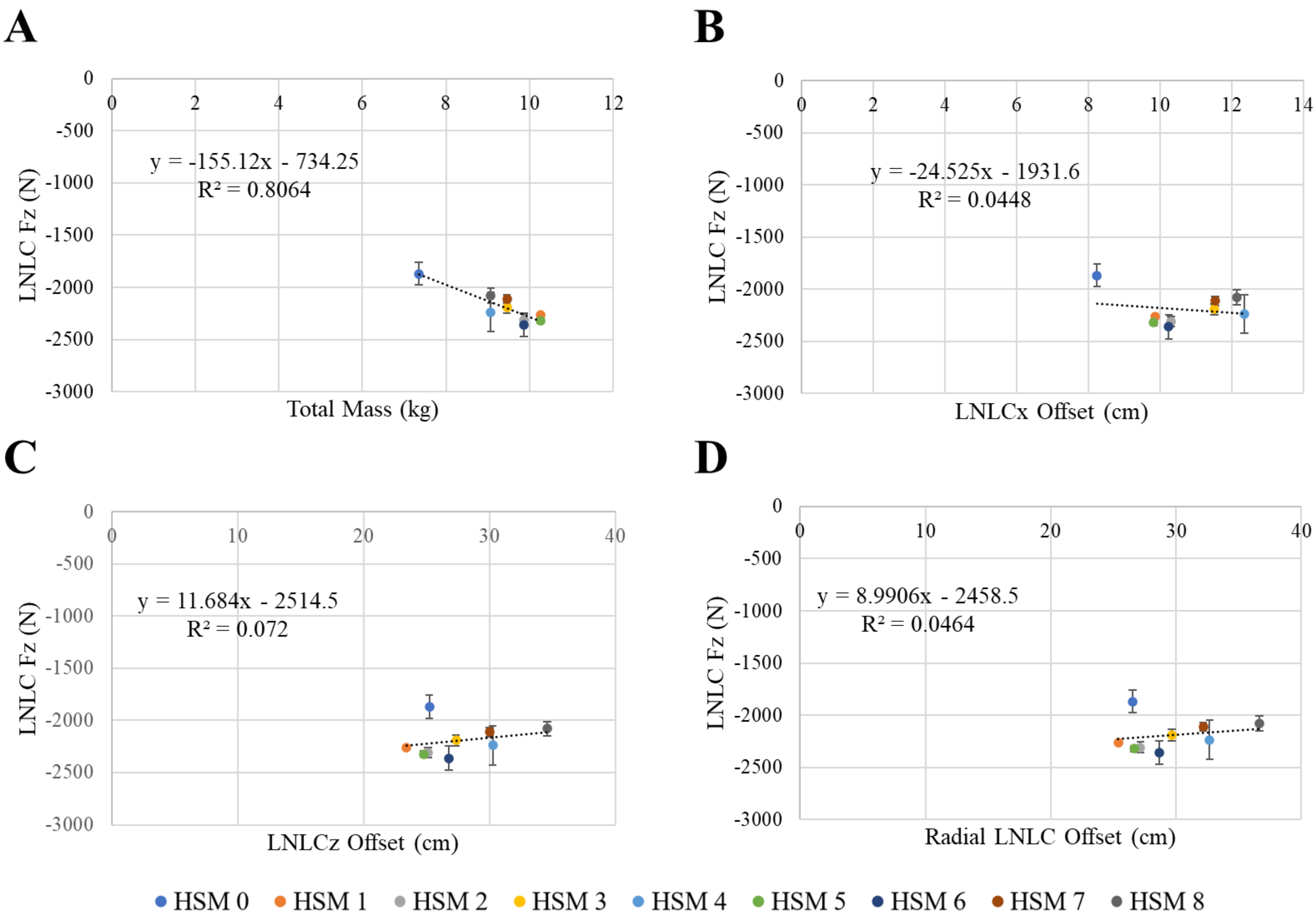

Figure A2. Scatter plots of LNLC F_z versus (A) total mass, (B) LNLCx offset, (C) LNLCz offset, and (D) radial LNLC offset in the thrust phase were produced.

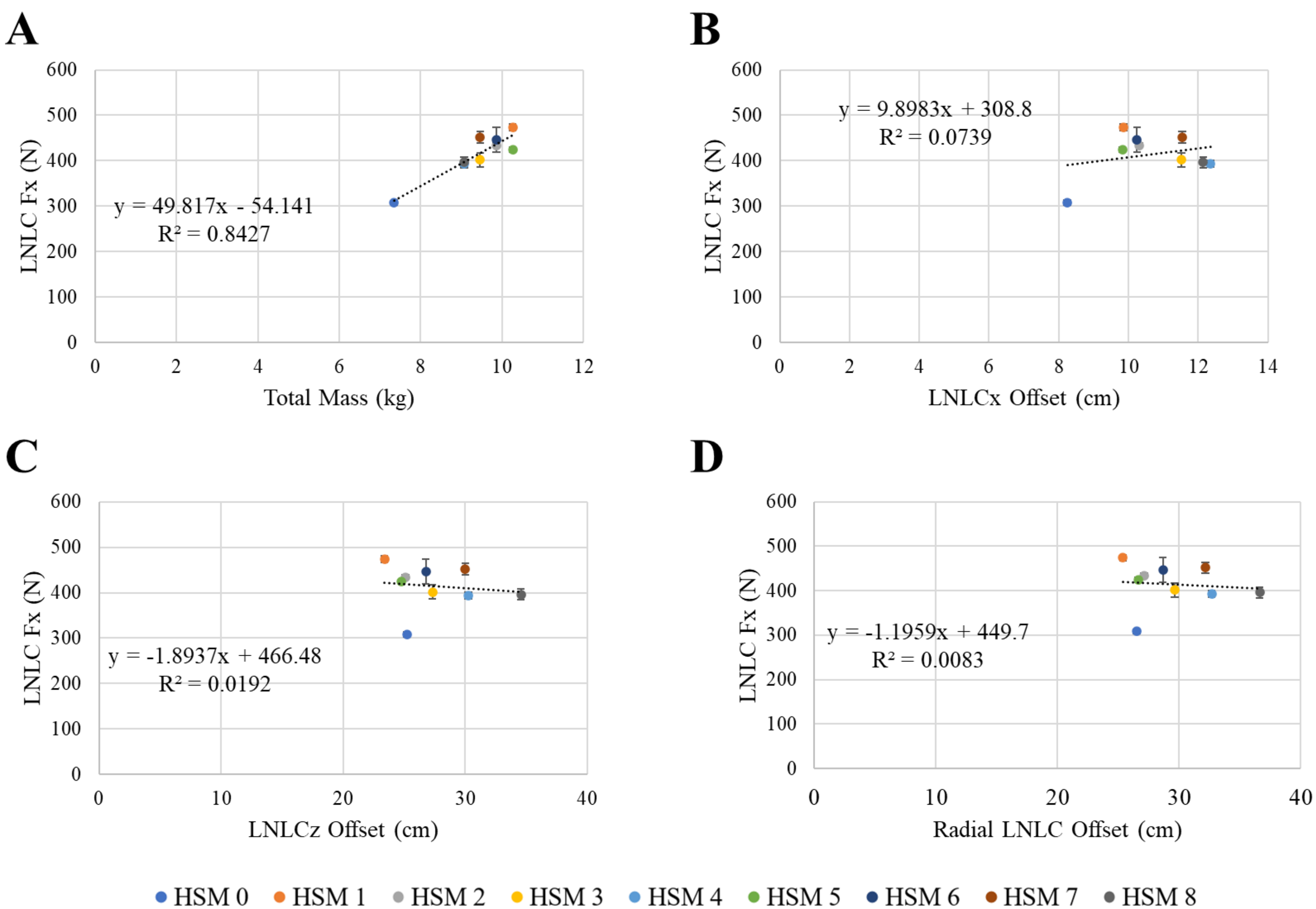

Figure A3. Scatter plots of LNLC F_x versus (A) total mass, (B) LNLCx offset, (C) LNLCz offset, and (D) radial LNLC offset in the thrust phase were produced.

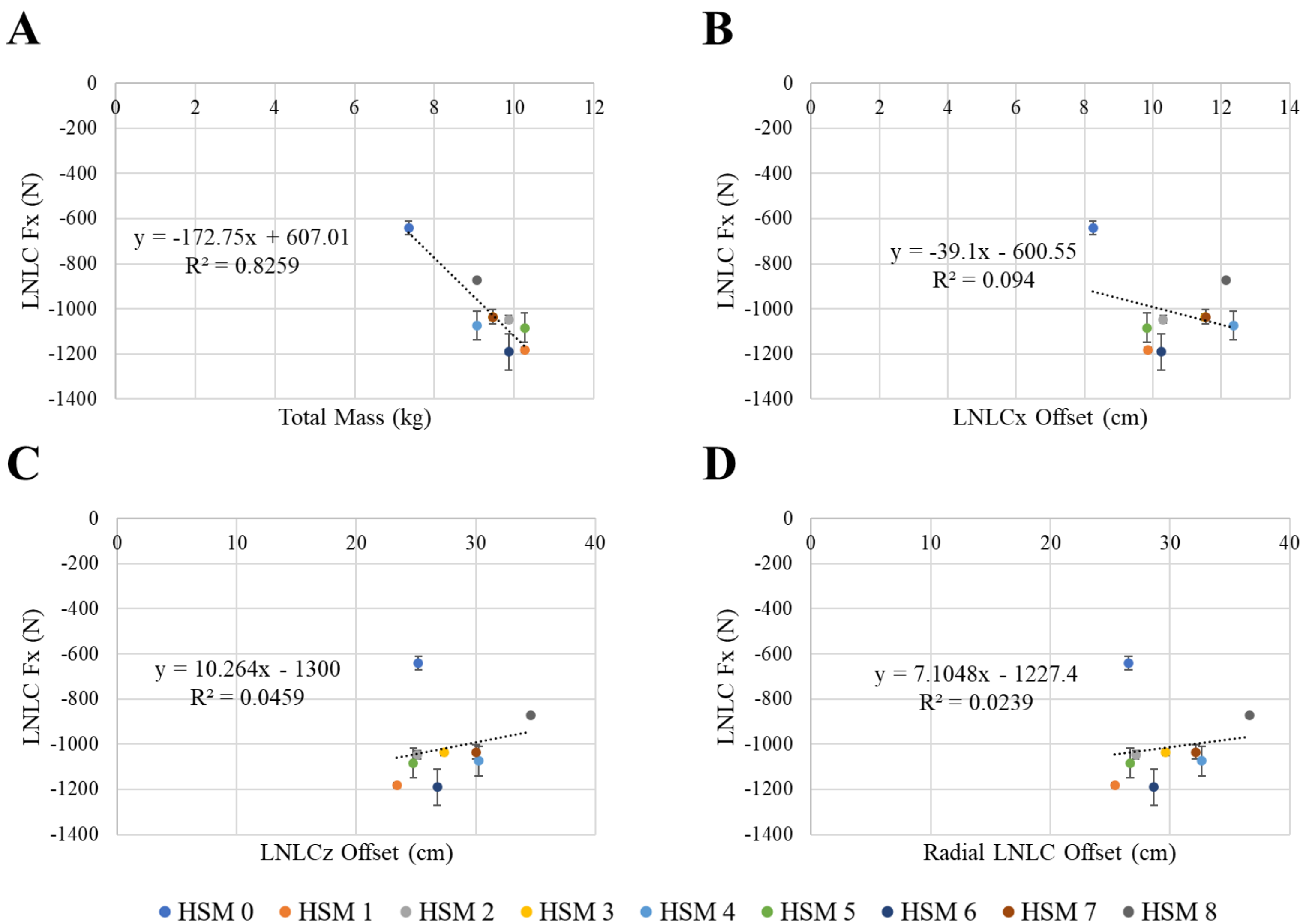

Figure A4. Scatter plots of LNLC F_x versus (A) total mass, (B) LNLCx offset, (C) LNLCz offset, and (D) radial LNLC offset in the thrust phase were produced.

Appendix B. Flail Data

Table B1. Averaged Comparison of UNLC Data for CMG1 and CMG2 Conditions for the Flail Phase

HSM	Flail F_x		Flail F_z		Flail M_y		Nij Flail	
	N	StD	N	StD	N-m	StD	Nij	StD
HSM0	-437.3	17.3	405.2	9.8	1093.4	159.7	0.184	0.006
HSM1	**-675.7**	19.1	818.5	10.7	1136.5	170.8	0.173	0.002
HSM2	-612.1	5.3	721.1	10.7	1370.1	142.3	0.155	0.001
HSM3	-597.4	33.8	689.9	33.8	1493.3	153.0	0.151	0.001
HSM4	-613.4	22.2	857.2	157.0	**2082.2**	445.7	0.175	0.023
HSM5	-627.2	17.8	763.8	67.2	1409.6	281.6	0.165	0.007
HSM6	-653.0	18.7	**935.9**	149.9	1682.8	260.2	**0.190**	0.026
HSM7	-619.6	15.6	713.9	23.1	1632.1	102.8	0.158	0.004
HSM8	-487.5	10.7	622.3	12.9	1827.8	69.4	0.157	0.01

Note 1. Largest values of the flail phase are in bold red font.
Note 2. CMG0 (HSM0) is shaded gray. CMG1 (HSM1 through HSM4) and CMG2 (HSM5 through HSM8) are shaded yellow and blue, respectively.

Table B2. Averaged Comparison of LNLC Data for CMG1 and CMG2 Conditions for the Flail Phase

HSM	Flail F_x		Flail F_z		Flail M_y		BC Flail	
	N	StD	N	StD	N-m	StD	BC	StD
HSM0	-641.4	37.8	405.7	24.5	5684.8	241.5	0.437	0.862
HSM1	**-1180.6**	13.3	**451.5**	13.8	8617.1	35.6	1.225	0.006
HSM2	-1046.2	22.2	384.8	23.1	8527.2	196.6	1.219	0.021
HSM3	-1036.9	17.8	405.7	17.8	8631.3	334.1	1.200	0.041
HSM4	-1073.8	79.6	427.9	40.9	8258.6	447.0	1.225	0.012
HSM5	-1084.0	79.2	392.3	21.8	7798.2	450.6	1.128	0.042
HSM6	-1190.8	97.0	438.6	46.3	8255.5	774.4	1.237	0.047
HSM7	-1034.7	38.3	383.4	39.6	**8978.3**	298.0	**1.259**	0.030
HSM8	-871.0	5.3	277.6	9.3	7937.0	235.8	1.174	0.021

Note 1. Largest values of the flail phase are in bold red font.
Note 2. CMG0 (HSM0) is shaded gray. CMG1 (HSM1 through HSM4) and CMG2 (HSM5 through HSM8) are shaded yellow and blue, respectively.

Table B3. Averaged Comparison of UNLC Data for CMG0, CMG1, and CMG2 Conditions for the Flail Phase

HSM Condition	Nij	StD
HSM0	0.184	0.006
HSM1	0.173	0.002
HSM2	0.155	0.001
HSM3	0.151	0.001
HSM4	0.175	0.023
HSM5	0.165	0.007
HSM6	**0.190**	0.026
HSM7	0.158	0.004
HSM8	0.157	0.01

Note 1. Largest Nij value of the flail phase is in bold red font.
Note 2. CMG0 (HSM0) is shaded gray. CMG1 (HSM1 through HSM4) and CMG2 (HSM5 through HSM8) are shaded yellow and blue, respectively.

Table B4. Averaged Comparison of LNLC Data for CMG0, CMG1, and CMG2 Conditions for the Flail Phase

HSM Condition	BC	StD
HSM0	0.437	0.862
HSM1	1.225	0.006
HSM2	1.219	0.021
HSM3	1.200	0.041
HSM4	1.225	0.012
HSM5	1.128	0.042
HSM6	1.237	0.047
HSM7	**1.259**	0.030
HSM8	1.174	0.021

Note 1. Largest BC value of the flail phase is in bold red font.
Note 2. CMG0 (HSM0) is shaded gray. CMG1 (HSM1 through HSM4) and CMG2 (HSM5 through HSM8) are shaded yellow and blue, respectively.

Table B5. Percent Changes of Similar Vertical Offset Pairs for UNLC Data

Parameter	HSM2 & HSM5	HSM3 & HSM6	HSM4 & HSM7
Thrust F_x	-9.1%	**14.6%***	3.4%
Thrust F_z	0.9%	5.9%	2.3%
Thrust M_y	2.8%	**11.8%**	**15.2%**
Flail F_x	2.5%	9.3%*	1.0%
Flail F_z	5.9%	**35.7%***	**-16.7%**
Flail M_y	2.9%	12.7%	**-21.6%**
Nij Thrust Max	2.4%	1.4%	5.1%
Nij Flail Max	6.4%	**25.9%**	-9.7%

Note. Percent differences larger that ± 10% are in bold red font.
*Statistically significant difference with *p*-value < 0.05

Table B6. Percent Changes of Vertical Offset Pairs for LNLC Data

Parameter	HSM2 & HSM5	HSM3 & HSM6	HSM4 & HSM7
Thrust F_x	-2.1%	**11.1%**	**14.9%***
Thrust F_z	0.5%	7.7%	-5.6%
Thrust M_y	6.5%	3.3%	-2.6%
Flail F_x	3.6%	**14.8%**	-3.7%
Flail F_z	1.9%	8.1%	**-10.4%**
Flail M_y	-8.5%	-4.4%	8.7%
BC Thrust Max	**24.3%**	**-26.2%**	8.0%
BC Flail Max	-7.5%	3.0%	2.8%

Note. Percent differences larger that ± 10% are in bold red font.
*Statistically significant difference with *p*-value < 0.05

This space is intentionally blank.

Table B7. Average Nij, StD, and Percent Change for All CMGs in the Flail Phase

CMG Condition	Average	StD
CMG0	0.18	0.01
CMG1	0.16	0.01
CMG2	0.17	0.02
CMG Condition Comparison	**% Change**	**Tukey Test (*p*-value)**
CMG1 to CMG0	-11%	NA*
CMG2 to CMG0	-6%	NA*
CMG2 to CMG1	6%	NA*

*ANOVA was not significant.

Table B8. Average BC, StD, and Percent Difference for All CMGs in the Flail Phase

CMG Condition	Avg	StD
CMG0	0.89	0.02
CMG1	1.22	0.02
CMG2	1.20	0.06
CMG Condition Comparison	**% Change**	**Tukey Test (*p*-value)**
CMG1 to CMG0	37%	0.014
CMG2 to CMG0	35%	0.044
CMG2 to CMG1	-1%	0.488

Table B9. Average, StD, and % Change in Peak UNLC M_y, F_z, and F_x for All CMG in the Flail Phase

CMG Condition	M_y (N-m)		F_z (N)		F_x (N)	
	Avg	StD	Avg	StD	Avg	StD
CMG0	3.14	0.37	1801.68	35.39	-1944.92	63.65
CMG1	4.36	1.17	3432.45	418.13	-2778.23	7.93
CMG2	4.70	0.64	3376.31	590.46	-2655.00	14.77
CMG Condition Comparison	**% Change**	***p*-value**	**% Change**	***p*-value**	**% Change**	***p*-value**
CMG1 to CMG0	39%		91%	<0.001	43%	<0.001
CMG2 to CMG0	50%	NA*	87%	<0.001	37%	<0.001
CMG2 to CMG1	8%		-2%	0.961	-4%	0.419

*ANOVA was not significant.

Table B10. Average, StD, and % Change in Peak LNLC M_y, F_z, and F_x for All CMG in the Flail Phase

CMG Condition	**M_y (N-m)**		**F_z (N)**		**F_x (N)**	
	Avg	**StD**	**Avg**	**StD**	**Avg**	**StD**
CMG0	144.39	5.01	405.51	20.02	-641.29	31.05
CMG1	24.42	0.82	417.45	32.66	-4823.75	15.04
CMG2	23.65	1.74	373.06	64.67	-4649.35	28.57
CMG Condition Comparison	**% Change**	***p*-value**	**% Change**	***p*-value**	**% Change**	***p*-value**
CMG1 to CMG0	-83%	<0.001	3%		652%	<0.001
CMG2 to CMG0	-84%	<0.001	-8%	NA*	625%	<0.001
CMG2 to CMG1	-3%	0.375	-11%		-4%	0.621

*ANOVA was not significant.

This space is intentionally blank.

This space is intentionally blank.

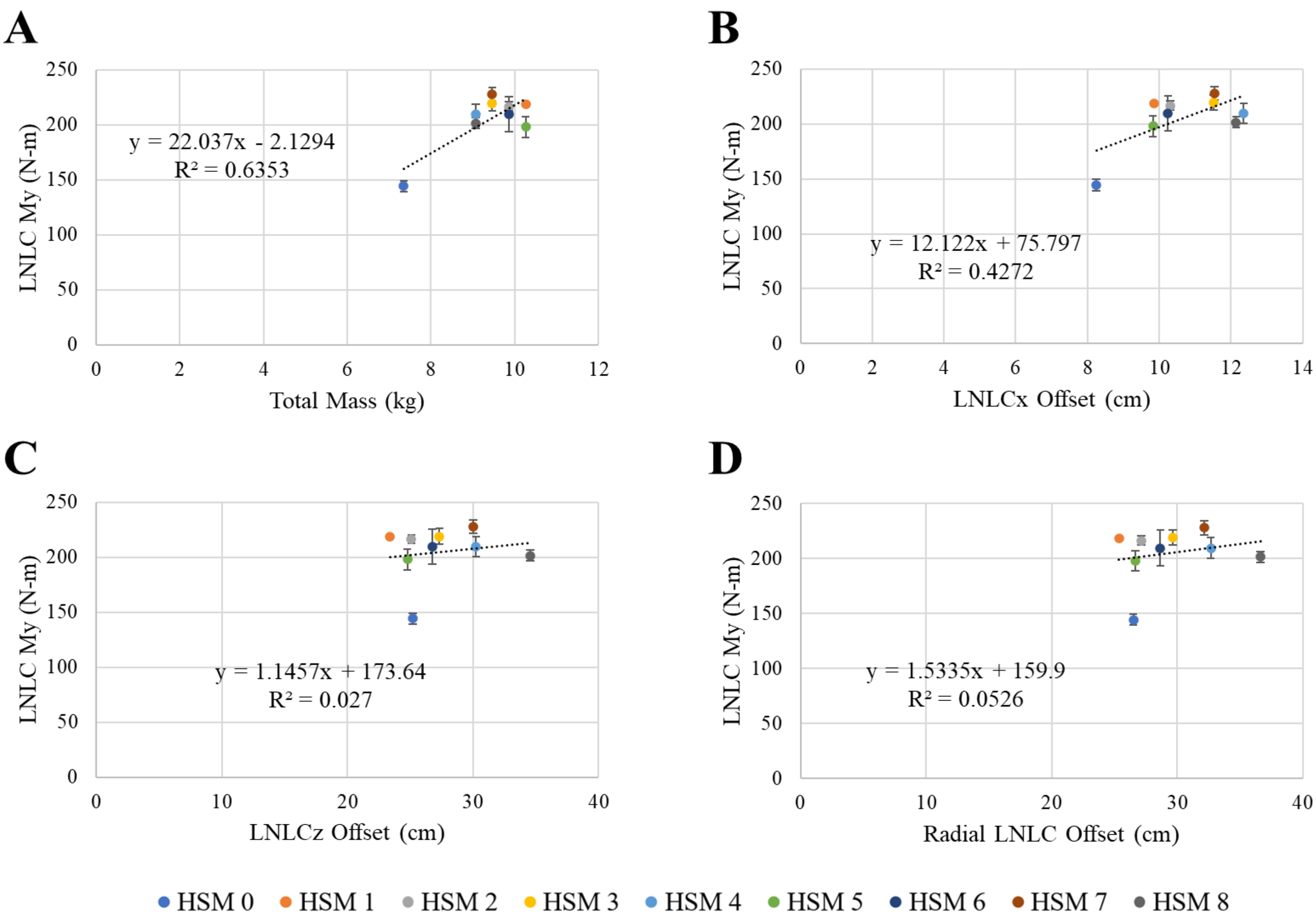

Figure B1. Scatter plots of LNLC M_y versus (A) total mass, (B) LNLCx offset, (C) LNLCz offset, and (D) radial LNLC offset in the flail phase were produced.

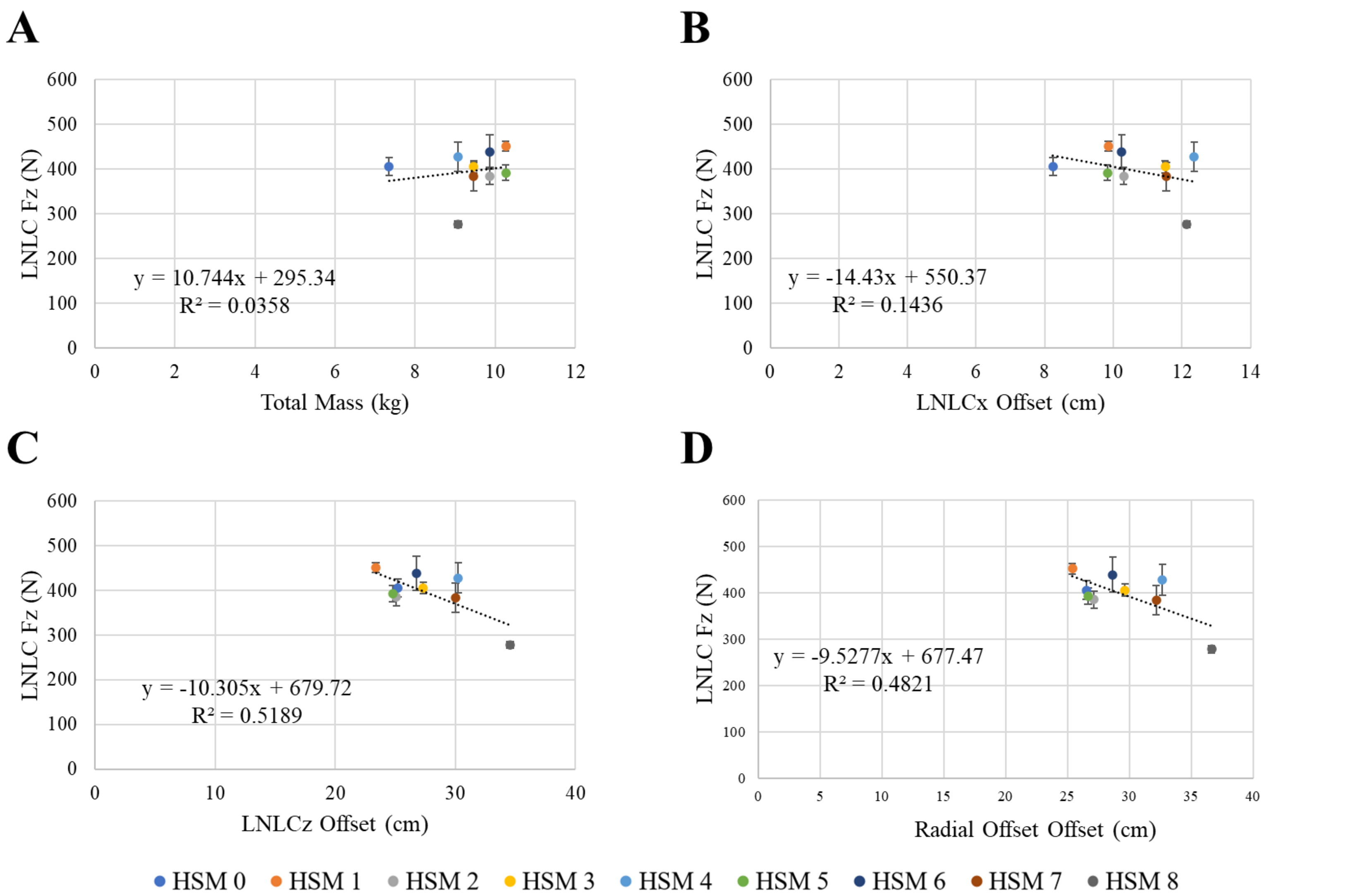

Figure B2. Scatter plots of LNLC F_z versus (A) total mass, (B) LNLCx offset, (C) LNLCz offset, and (D) radial LNLC offset in the flail phase were produced.

Table B11. Averaged Nij Data for HSM Configurations Listed from Largest to Smallest Radial LNLC Offset for the Flail Phase

HSM Condition	Radial LNLC offset (cm)	Nij	StD
HSM8	**10.14**	0.157	0.010
HSM4	6.50	0.175	0.023
HSM7	5.83	0.158	0.004
HSM3	3.89	0.151	0.001
HSM6	2.54	**0.190**	0.026
HSM1	2.43	0.173	0.002
HSM2	2.06	0.155	0.001
HSM5	1.63	0.165	0.007
HSM0	0	0.184	0.006

Note 1. Largest values of each parameter are in bold red font.
Note 2. CMG0 (HSM0) is shaded gray. CMG1 (HSM1 through HSM4) and CMG2 (HSM5 through HSM8) are shaded yellow and blue, respectively.

This space is intentionally blank.

Table B12. Averaged BC Data for HSM Configurations Listed from Largest to Smallest Radial LNLC offset for the Flail Phase

HSM Condition	Radial LNLC offset (cm)	BC	StD
HSM8	**10.14**	1.174	0.021
HSM4	6.50	1.225	0.012
HSM7	5.83	**1.259**	0.030
HSM3	3.89	1.200	0.041
HSM6	2.54	1.237	0.047
HSM1	2.43	1.225	0.006
HSM2	2.06	1.219	0.021
HSM5	1.63	1.128	0.042
HSM0	0	0.437	0.862

Note 1. Largest values of each parameter are in bold red font.
Note 2. CMG0 (HSM0) is shaded gray. CMG1 (HSM1 through HSM4) and CMG2 (HSM5 through HSM8) are shaded yellow and blue, respectively.

Table B13. Flail Phase Linear Regression Model Results for the Dependent Variables

Flail Phase	LNLC M_y ($R^2 = 0.692$; *p*-value < 0.001)		LNLC F_z ($R^2 = 0.390$; *p*-value $= 0.003$)		LNLC F_x ($R^2 = 0.768$; *p*-value < 0.001)	
	Coefficient	***p*-value**	**Coefficient**	***p*-value**	**Coefficient**	***p*-value**
Constant	-10.678	0.038	635.215	<0.001	2734.328	0.022
Total Mass	2.698	<0.001	3.966	0.702	-769.095	<0.001
Radial LNLC Offset	0.287	0.005	-9.360	<0.001	-0.942	0.965

Table B14. The R^2 of Each Independent and Dependent Variables for Thrust and Flail Phases

Output Variable	Flail LNLC M_y	LNLC F_z	LNLC F_x
Total Mass	0.64	0.04	**0.83**
LNLCx Offset	0.43	0.14	0.09
LNLCz Offset	0.03	0.52	0.05
Radial LNLC Offset	0.05	0.48	0.02

Note. Strong correlations are in bold red font.

U.S. ARMY AEROMEDICAL RESEARCH LABORATORY

FORT RUCKER, ALABAMA

Optimizing

HUMAN PROTECTION AND PERFORMANCE

since 1962

U.S. ARMY

FCC

MRDC